

Protected Radio Frequencies

Radio Quiet Zones around Observatories

US246 : No station shall be authorized to transmit in the following bands:

- 73-74.6 MHz,
- 608-614 MHz, except for medical telemetry equipment,
- 1400-1427 MHz,
- 1660.5-1668.4 MHz,
- 2690-2700 MHz,
- 4990-5000 MHz,
- 10.68-10.7 GHz,
- 15.35-15.4 GHz,
- 23.6-24 GHz,
- 31.3-31.8 GHz,
- 50.2-50.4 GHz,
- 52.6-54.25 GHz,
- 86-92 GHz,
- 100-102 GHz,
- 109.5-111.8 GHz,
- 114.25-116 GHz,
- 148.5-151.5 GHz,
- 64-167 GHz,
- 182-185 GHz,
- 190-191.8 GHz,
- 200-209 GHz,
- 226-231.5 GHz,
- 250-252 GHz.

UNITED

STATES

FREQUENCY ALLOCATIONS

THE RADIO SPECTRUM

RADIO SERVICES COLOR LEGEND



ACTIVITY CODE



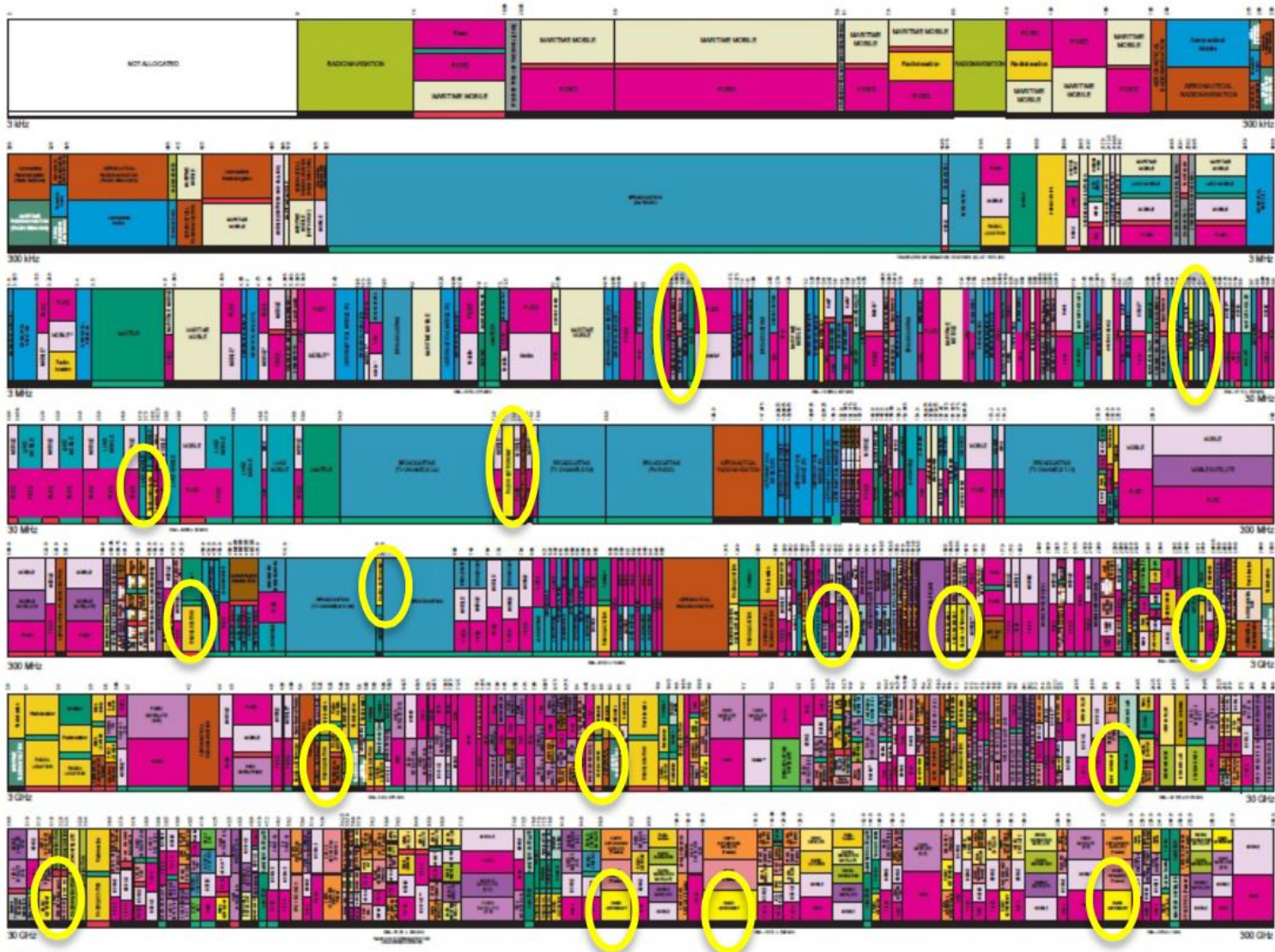
ALLOCATION USAGE DESIGNATION



THE SPECTRUM IS A LIMITED RESOURCE AND MUST BE USED IN AN EFFICIENT MANNER. THE FEDERAL COMMUNICATIONS COMMISSION (FCC) IS THE LEAD AGENCY FOR THE RADIO SPECTRUM. FOR MORE INFORMATION, VISIT [WWW.FCC.GOV](http://www.fcc.gov).



U.S. DEPARTMENT OF COMMERCE
National Telecommunications and Information Administration
Office of Spectrum Management
October 2009



For information on the radio spectrum, visit www.fcc.gov. For more information on the radio spectrum, visit www.fcc.gov.

Long Wavelength Limit

The refractive index of a cold neutral plasma is given by

$$\mu(\nu) = \sqrt{1 - \frac{\nu_p^2}{\nu^2}}, \quad (16.1.1)$$

where ν_p the “plasma frequency is given by

$$\nu_p = \sqrt{\frac{n_e e^2}{\pi m_e}} \simeq 9\sqrt{n_e} \text{ kHz} \quad (16.1.2)$$

where e is the charge on the electron, m_e is the mass of the electron and n_e is the electron number density (in cm^{-3}). At frequencies below the plasma frequency ν_p the refractive index becomes imaginary, i.e. the wave is exponentially attenuated and does not propagate through the medium. The earth’s ionosphere has electron densities $\sim 10^4 - 10^5 \text{ cm}^{-3}$, which means that the plasma frequency is $\sim 1 - 10 \text{ MHz}$. Radio waves with such low frequencies do not reach the earth’s surface and can be studied only by space based telescopes. The plasma between the planets is called the Interplanetary Medium (IPM) and has electron densities $\sim 1 \text{ cm}^{-3}$ (at the earth’s location); the corresponding cut off frequency is $\sim 9 \text{ kHz}$. The typical density in the Interstellar Medium (ISM) is $\sim 0.03 \text{ cm}^{-3}$ for which the cut off frequency is $\sim 1 \text{ kHz}$. Waves of such low frequency from extra solar system objects cannot be observed even by spacecraft since the IPM and ISM will attenuate them severely.

Atmospheric effects

- Background
- Extinction
- Differential refraction
- Seeing

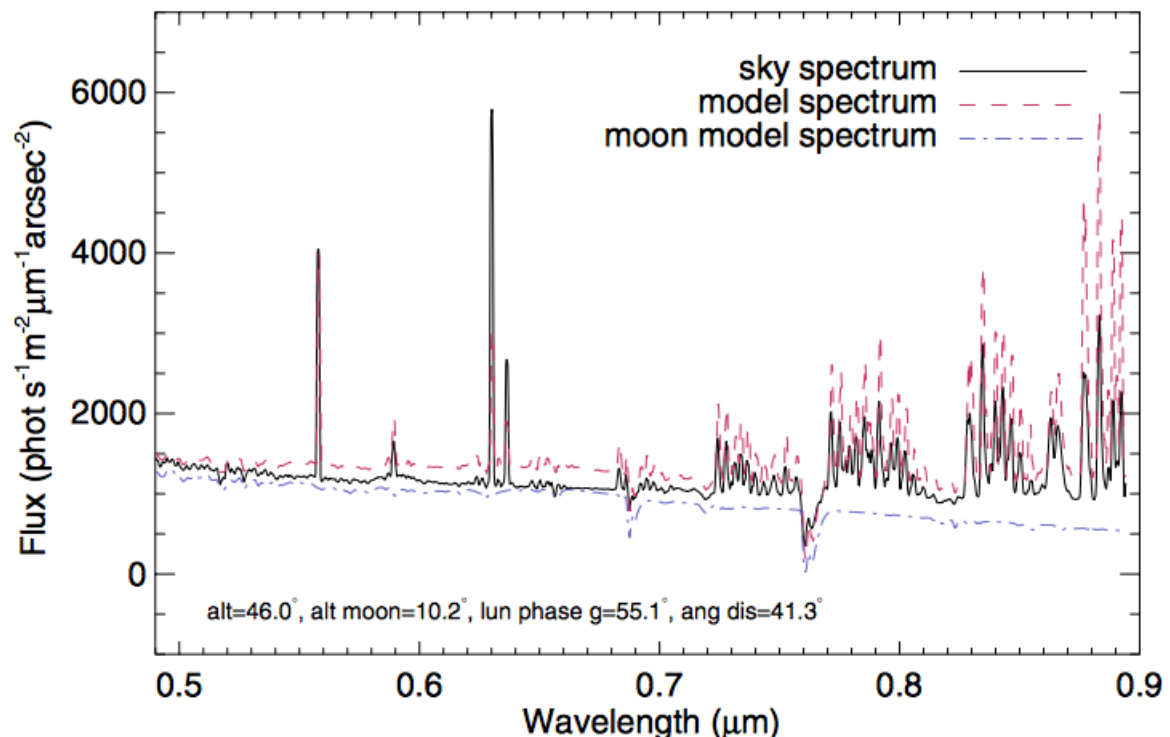
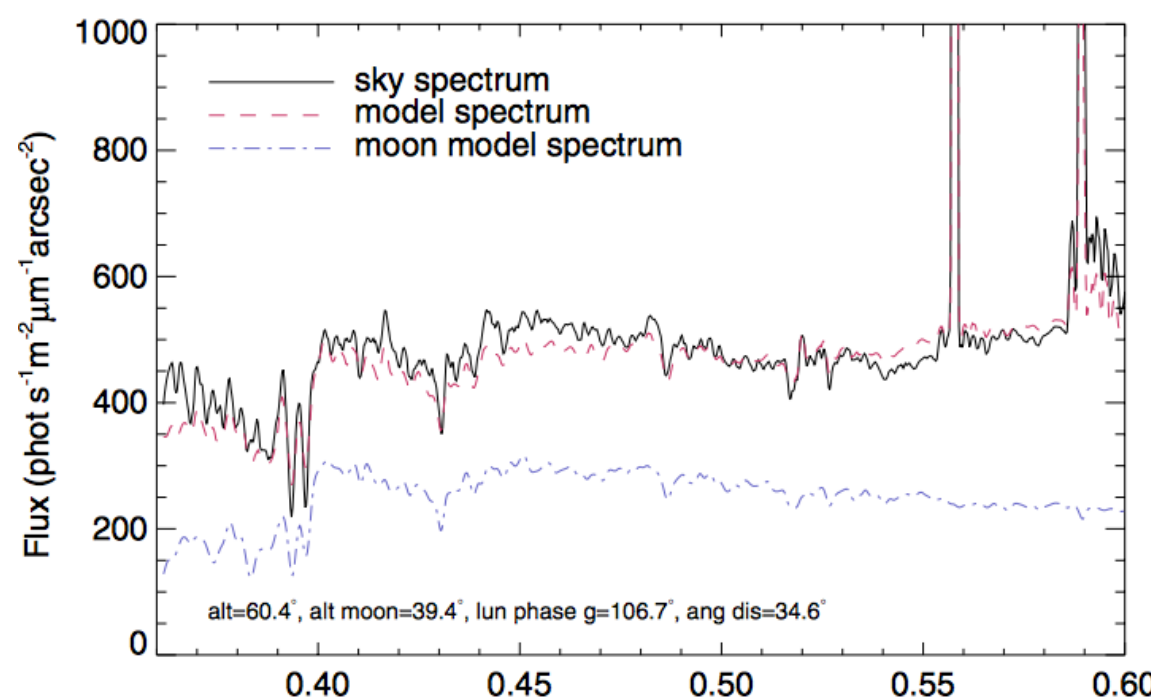
Atmospheric Background

Calculated sky brightness model compared with observations from FORS 1 at Paranal (A Jones et al 2013)

The two plots compare models with different contributions from scattered moonlight, which is the dominant source of background under bright sky conditions

The strong narrow features are OI] and NI airglow lines, which are variable, so intensities will not match a general model. OH emission becomes prominent longwards of 700nm

Note that the scattered light background is quite strongly polarized



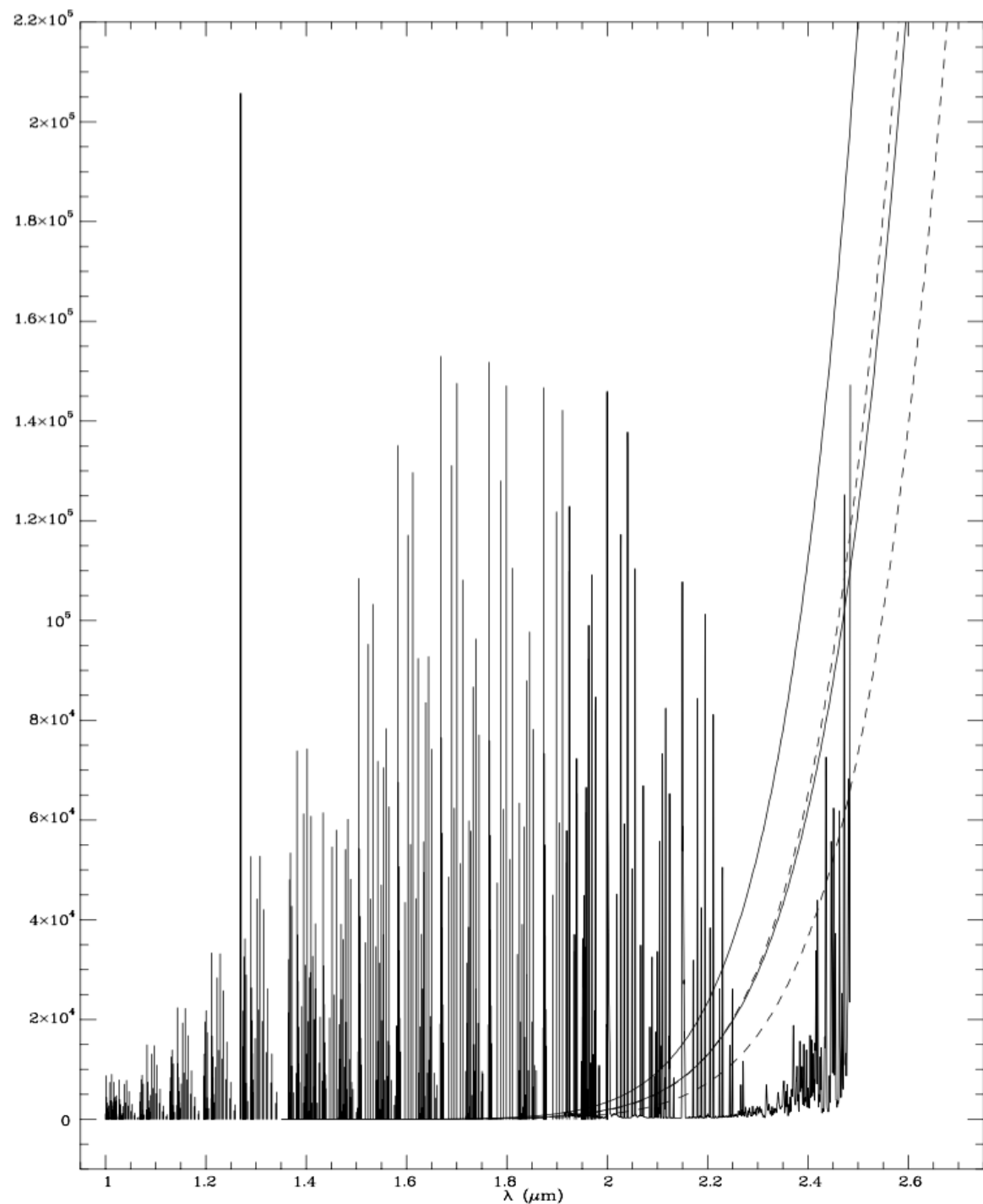
Near Infrared Sky Emission

Airglow lines from OH + O₂ emit strongly at far-red and near-IR wavelengths.

They are temporally and spatially variable and reduce sensitivity markedly.

Sites away from the geomagnetic poles are preferred

Model sky spectrum including airglow lines, thermal emission from the atmosphere with thermal emission from the telescope indicated by the continuous and dashed lines in summer and winter for high and low emissivities



Mid- Infrared Emission

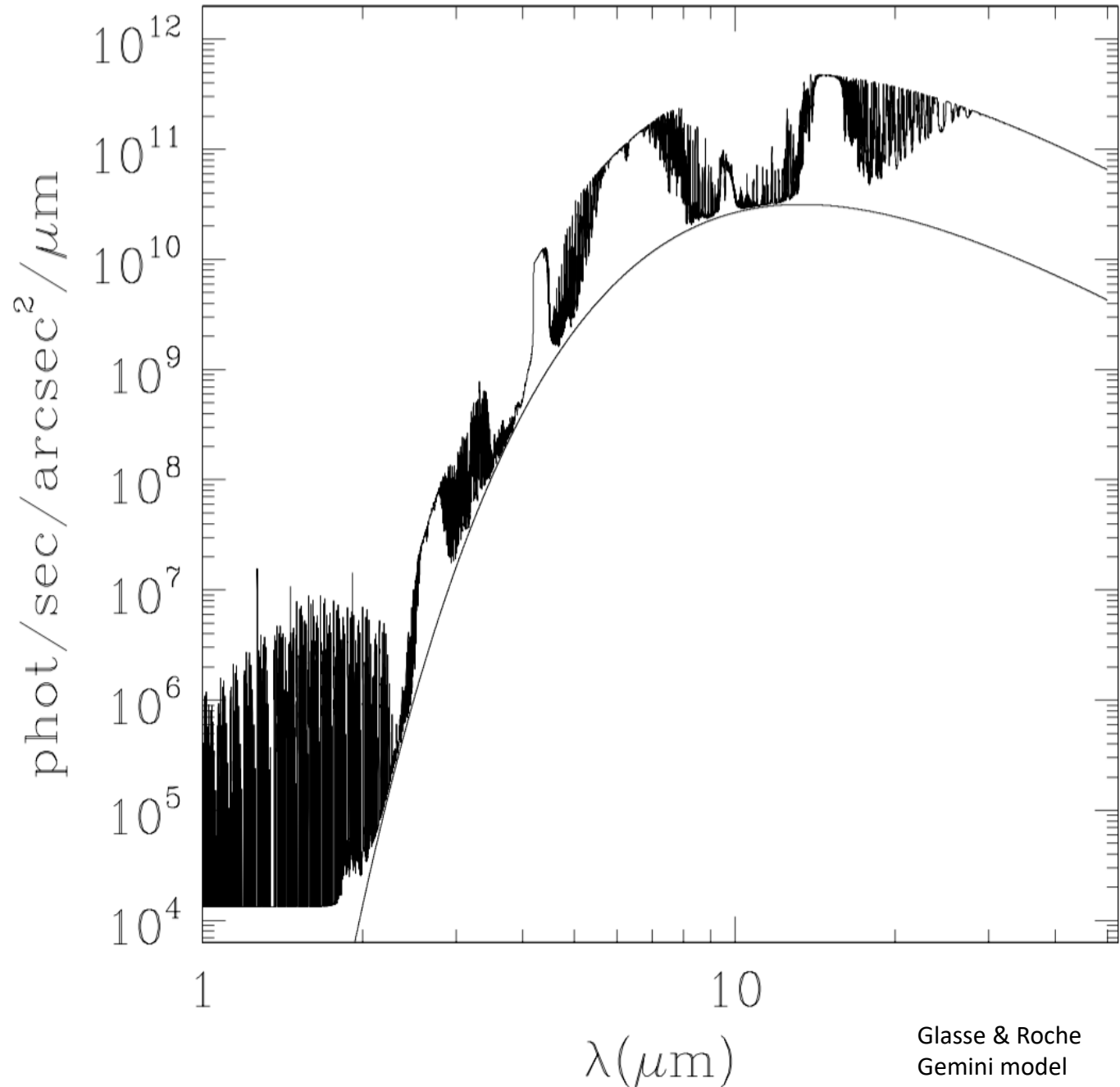
At mid-infrared wavelengths, the thermal emission from the sky dominates

It peaks at $\sim 12\mu\text{m}$ and leads to an enormous photon flux

Careful control of telescope emissivity and cold, dry sites are preferred.

In this model a telescope and sky temperature of 275K (winter on MK) is used with a system emissivity of 7%


MK 1.2mm PWV 275 K $e=7\%$



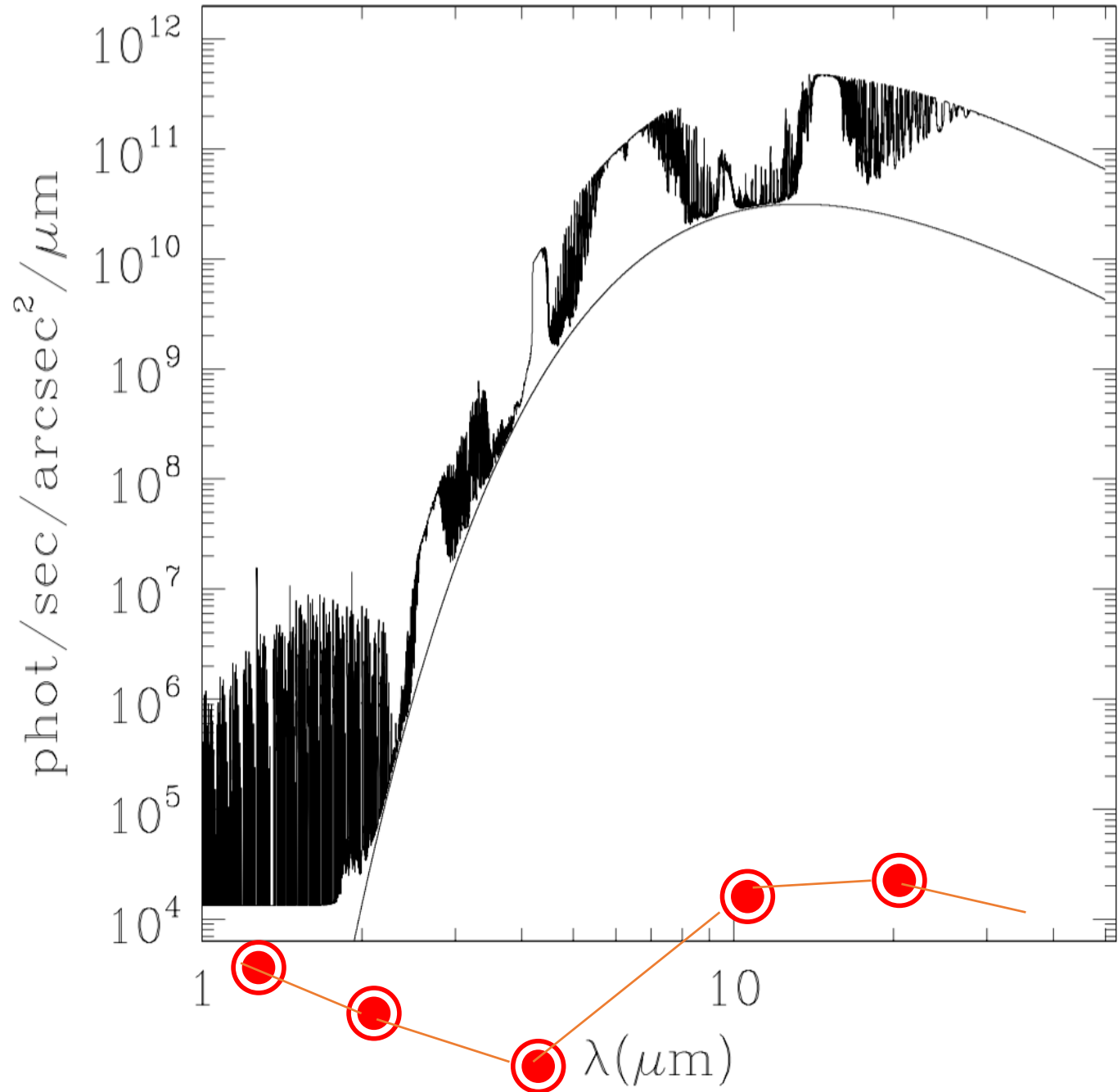
Mid- Infrared in Space

JWST is a passively cooled telescope at L2, launched in 2021

It is optimised for IR observations, taking advantage of the low sky background, and should be limited by zodiacal light from the solar system at $\lambda < 10\mu\text{m}$

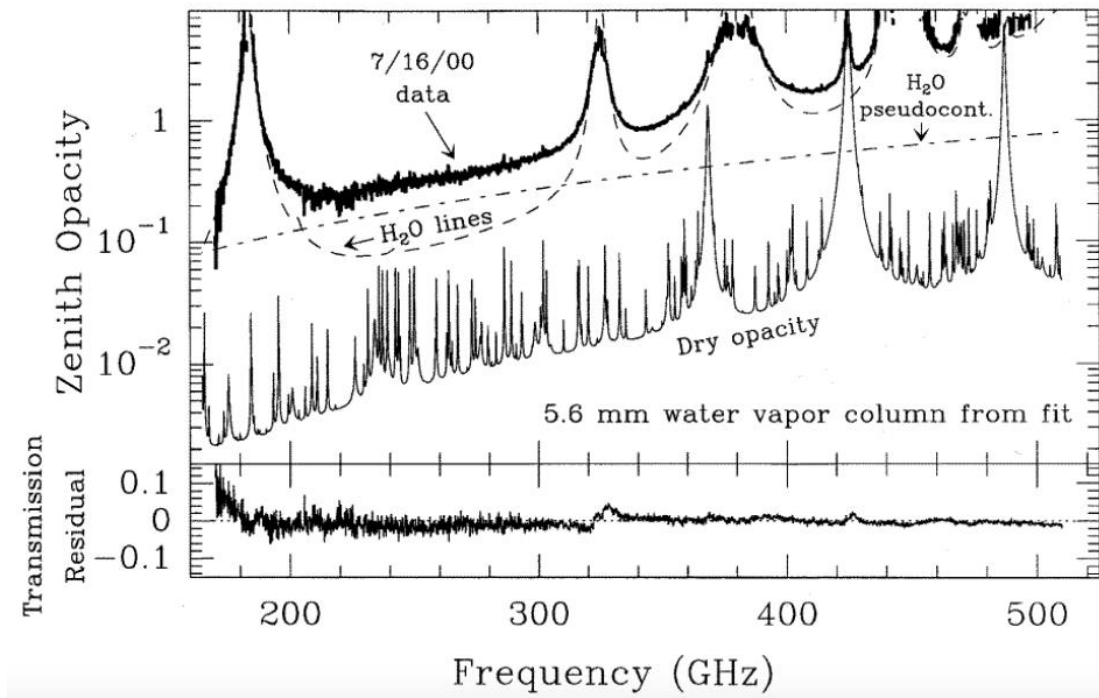
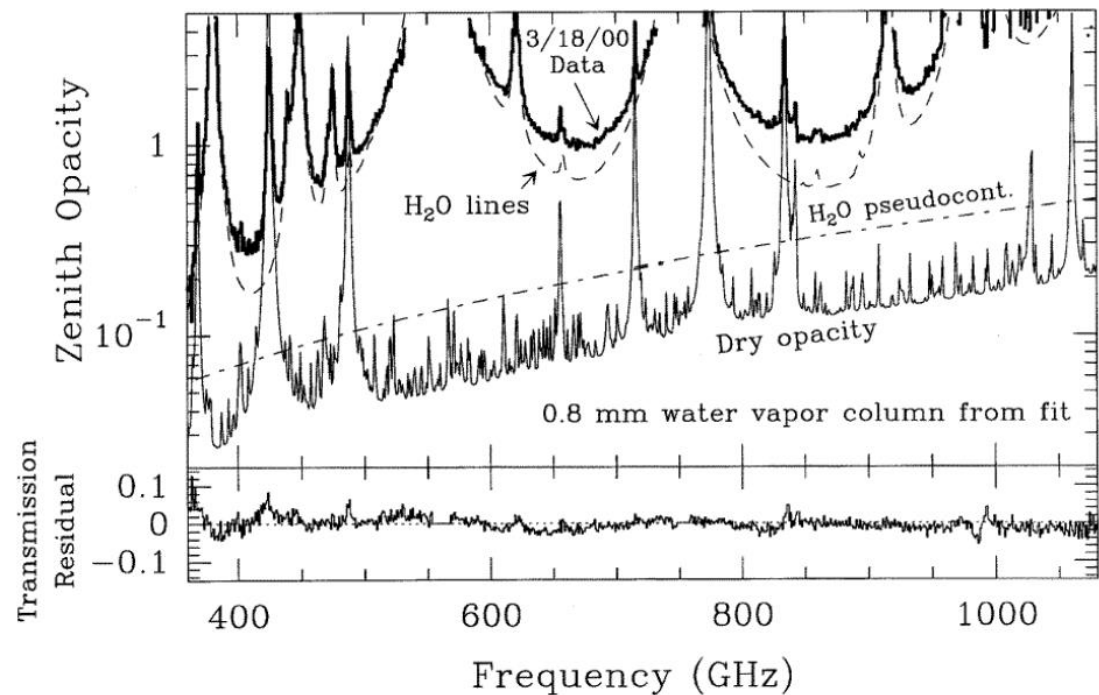
The photon background from the ZL at L2 is indicated by 

MK 1.2mm PWV 275 K $e=7\%$



Sub-mm Sky Emission at MK

- FTS zenith atmospheric opacity spectra obtained on Mauna Kea in March and July 2000 and best fit opacity contributions
- The fitting routine that produced these results is based on the radiative transfer code and uses only the precipitable water vapor column as a free parameter
(J R Pardo et al 2001)



Artificial Backgrounds

- City Lights,
- Dust
- Radio Frequency Interference
 - Broadcasts, mobile phones, microwaves, other equipment on site
- Satellites – reflected sunlight & comms
- Aircraft con trails etc
- Laser light from LGS
- + cosmic rays

- Plus Volcanic aerosols, Saharan dust etc

Optical/NIR Sky brightness values

Filter	Continuum brightness	
	[$\gamma/s/\mu m/m^2/arcsec^2$]	[mag/arcsec ²]
U	190	21.5
B	150	22.4
V	210	21.7
Rc	340	20.8
Ic	500	19.9
J	1200	18.0
H	2300	16.5
K	2300	15.7

Sky Brightness (mag/arcsec ²)					
lunar age (days)	U	B	V	R	I
0	22.0	22.7	21.8	20.9	19.9
3	21.5	22.4	21.7	20.8	19.9
7	19.9	21.6	21.4	20.6	19.7
10	18.5	20.7	20.7	20.3	19.5
14	17.0	19.5	20.0	19.9	19.2

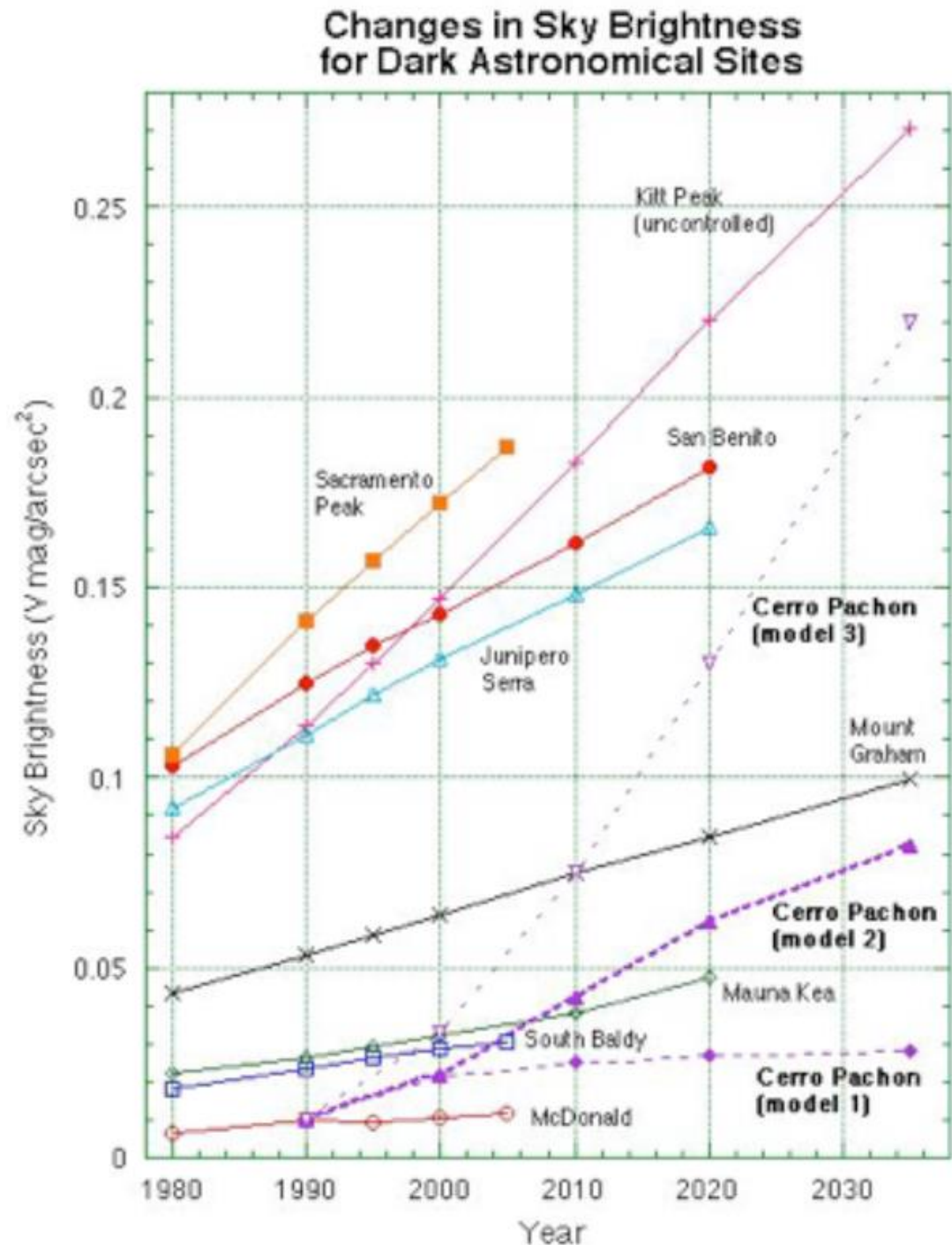
Paranal Sky Brightness at 3 days and variation with lunar phase

Dark Sky Protection

Threats from increasing populations, urban sprawl and Industrial developments

Education and Implementation and enforcement of Lighting Ordinances

Installation of light shields
Low pressure sodium lighting



Atmospheric Extinction under good conditions (Mauna Kea CFHT)

wavelength	mag/airmass	wavelength	mag/airmass
(nm)			
• 300	4.90	425	0.21
• 310	1.37	450	0.17
• 320	0.82	475	0.14
• 330	0.57	500	0.13
• 340	0.51	525	0.12
• 350	0.42	550	0.12
• 360	0.37	575	0.12
• 370	0.33	600	0.11
• 380	0.30	650	0.11
• 390	0.27	700	0.10
• 400	0.25	800	0.07
		900	0.05

IR Atmospheric Extinction under good conditions (Mauna Kea UKIRT)

Wavel/Filter	mean	median
	(mag/air mass)	(mag/air mass)
(0.36) U	0.358	0.358
(0.44) B	0.198 +/- 0.008	0.194
(0.55) V	0.119 0.005	0.111
(1.25) J	0.114 0.007	0.102
(1.65) H	0.068 0.006	0.059
(2.2) K	0.096 0.005	0.088
(3.4) L	0.203 0.030	0.150
(3.8) L'	0.112 0.009	0.093
(4.8) M	0.244 0.016	0.220
(10) N	0.184 0.017	0.151
(20) Q	0.503 0.030	0.451

Extinction Variations

- Mean or median extinction values are a useful guide, but the values to be used on a given night generally have to be calculated for the night.
- Thin cloud, dust etc can have a marked effect even on a usable night.

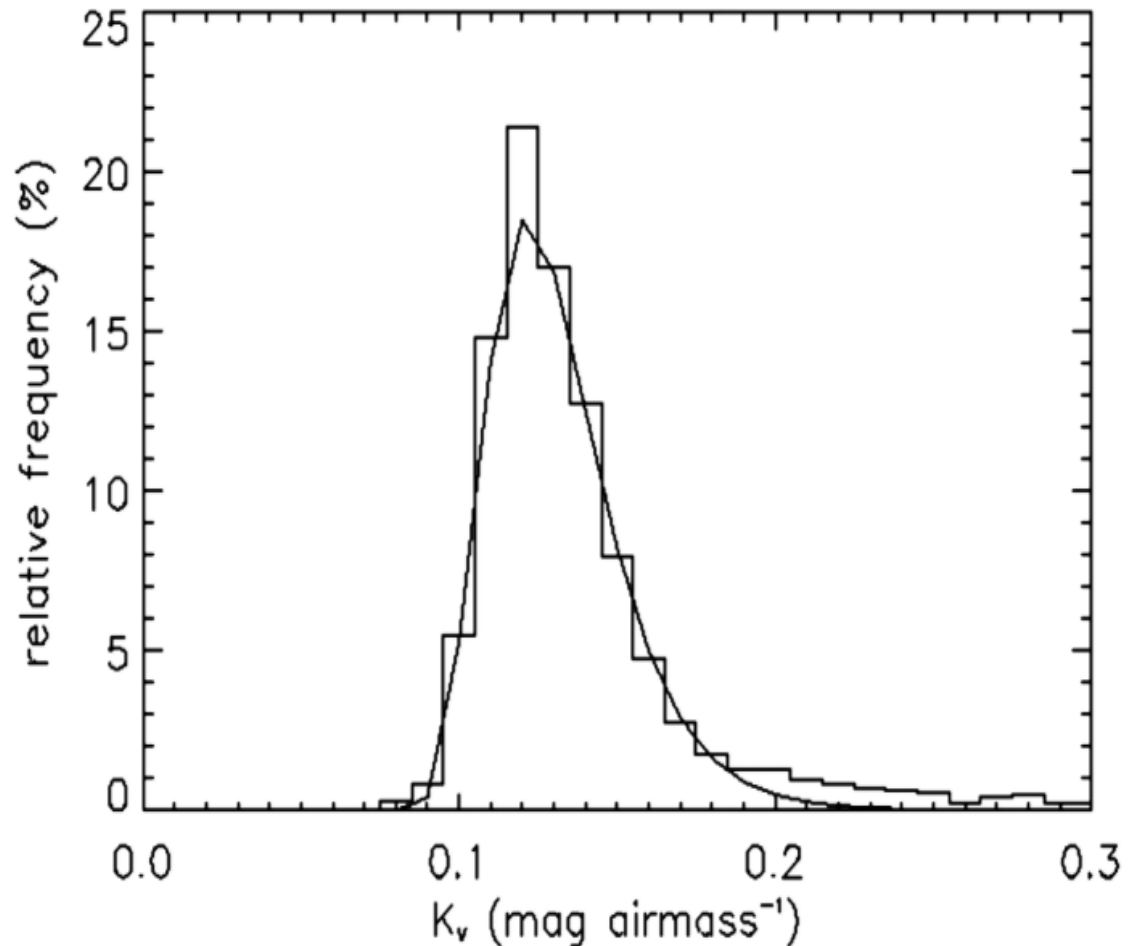
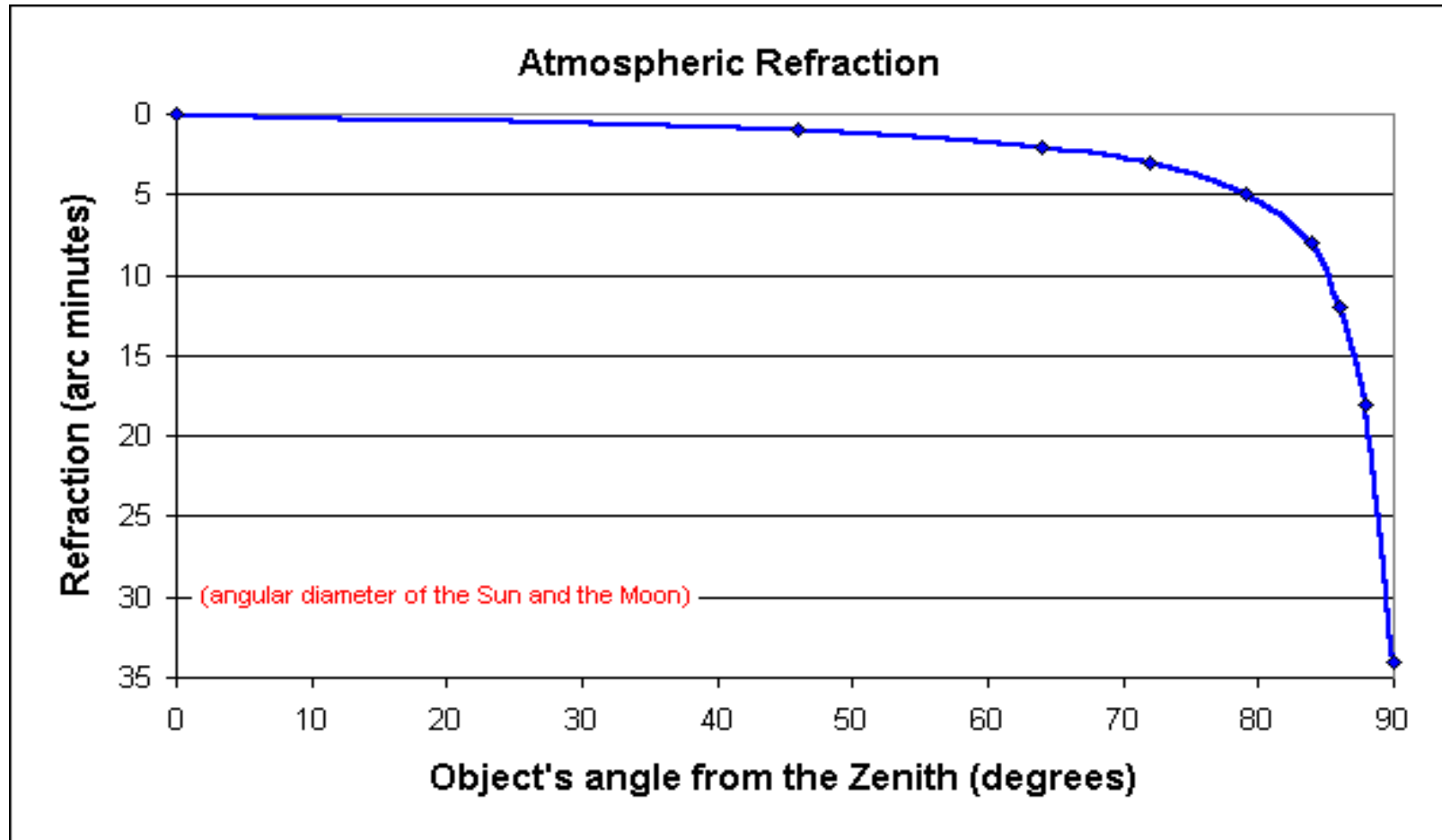


FIG. 7.—Histogram of the relative frequency of k_V for nonsummer nights V Band opacity for LaPalma over 20yr (A Garcia-Gil 2010)

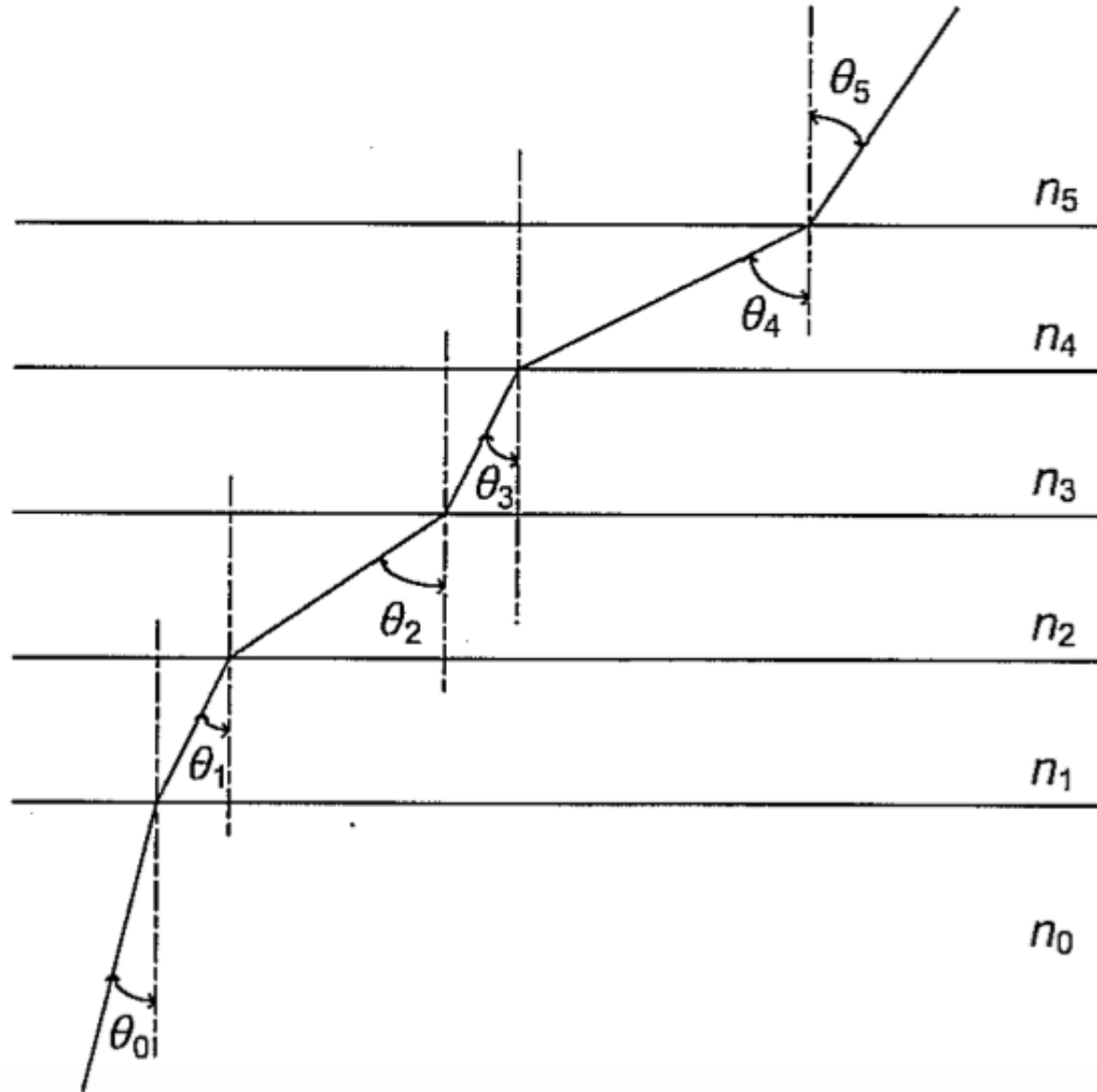
Atmospheric Refraction



- Observations made away from the zenith pass through atmospheric layers at an angle, leading to increasing refraction with zenith distance.

Refraction at different atmospheric layers

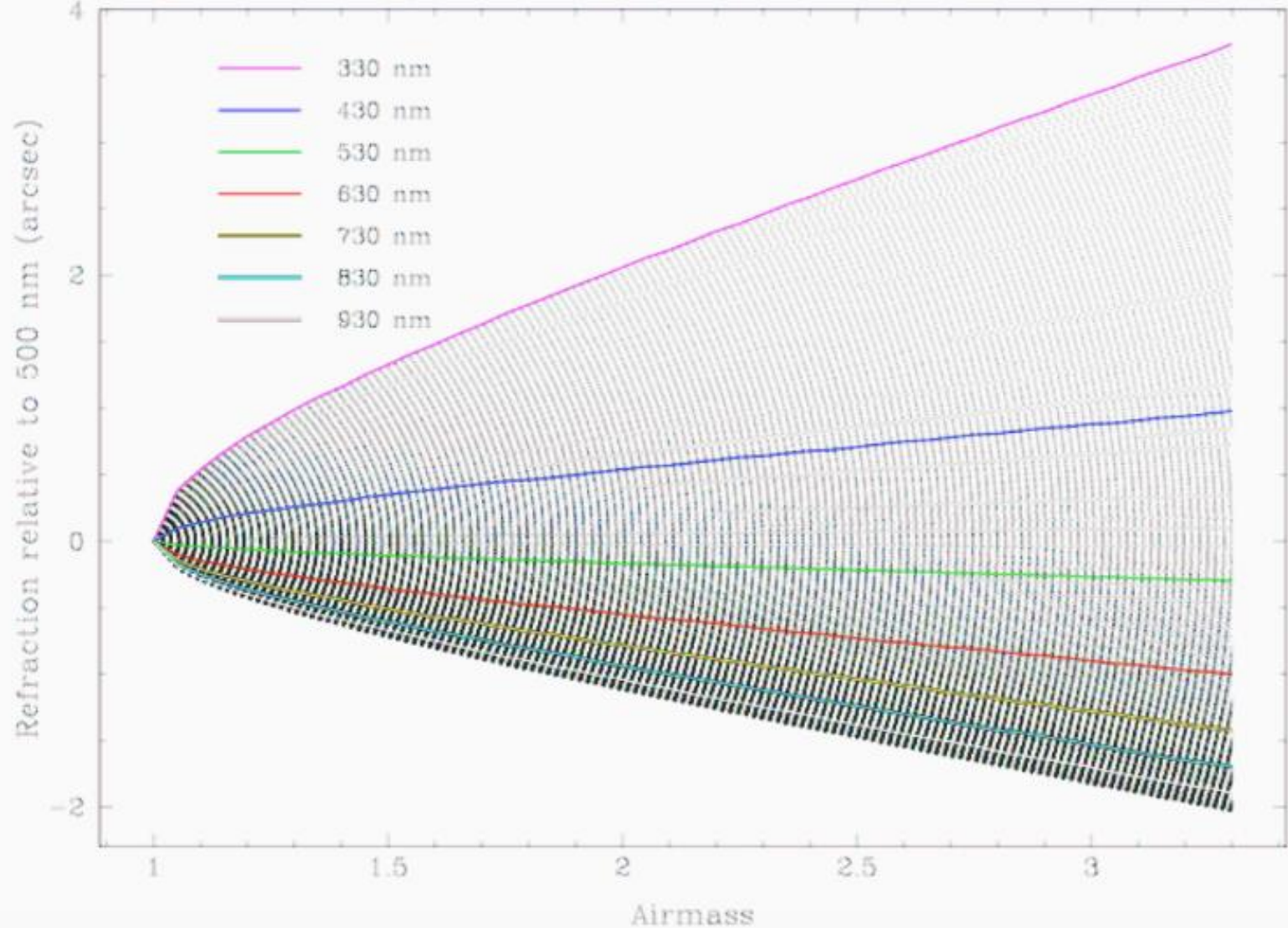
- Refraction at different atmospheric layers
- Accurate values require a full atmospheric model, taking account of P,T and n at different elevations



Atmospheric Refraction at Mauna Kea			
Zenith angle, degrees	Mauna Kea Table, arc seconds	Conventional theory, arc seconds	Lihue data, arc seconds
45°	36.70	36.80	36.81
50°	43.72	43.83	43.84
55°	52.35	52.47	52.50
60°	63.41	63.54	63.59
65°	78.35	78.48	78.56
70°	100.0	100.1	100.2
75°	134.7	134.7	135.0
80°	200.0	199.6	200.6
85°	361.8	361.6	366.5

TABLE OF ATMOSPHERIC REFRACTION AT THE MAUNA KEA OBSERVATORY, FOR $\lambda = .633$ MICRONS. THE FIRST COLUMN ARE OBSERVATIONS ANGLES RELATIVE TO THE OBSERVER'S ZENITH. THE SECOND COLUMN IS A REFRACTION TABLE AT THE MAUNA KEA OBSERVATORY. THE THIRD COLUMN WAS CALCULATED FROM THE CONVENTIONAL PARAMETERS. THE FOURTH COLUMN WAS CALCULATED FROM A LEAST SQUARES FIT TO THE LIHUE DATA FOR THE RATIO PRESSURE/TEMPERATURE DEPENDENCE ON ALTITUDE. IN KAUAI, ON AUGUST 20,2016.

Differential Atmospheric Refraction on Mauna Kea (330 nm – 1.03 μm)



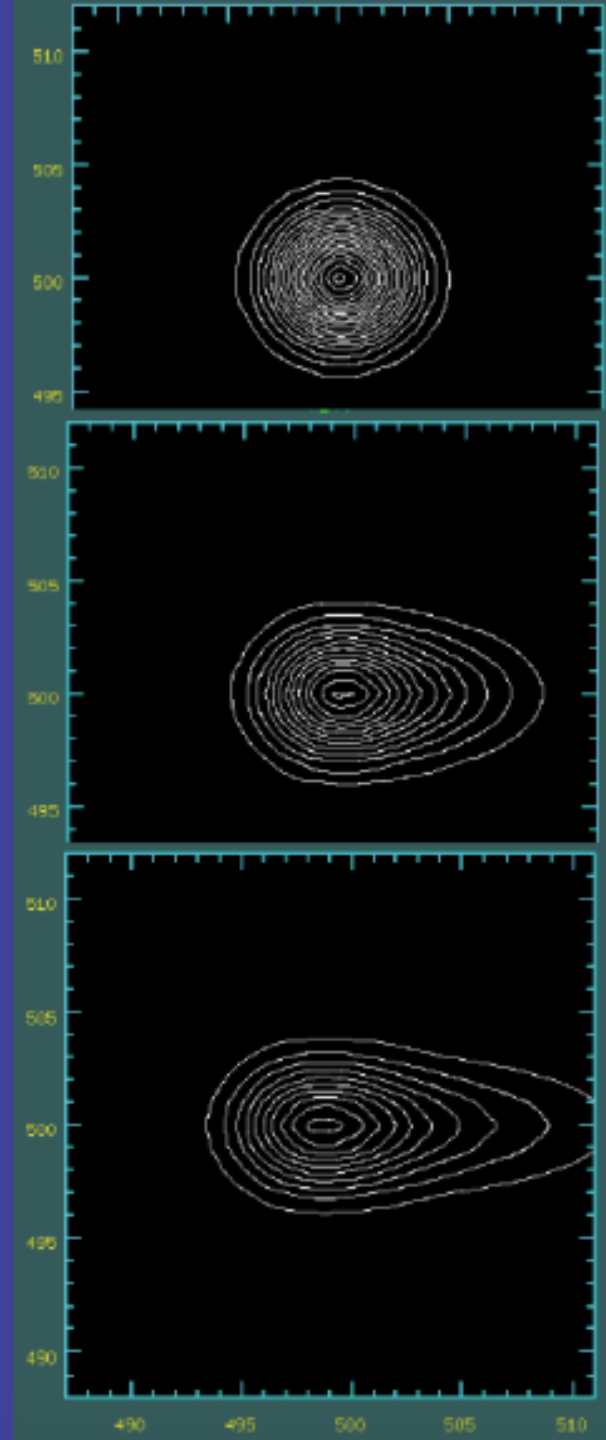
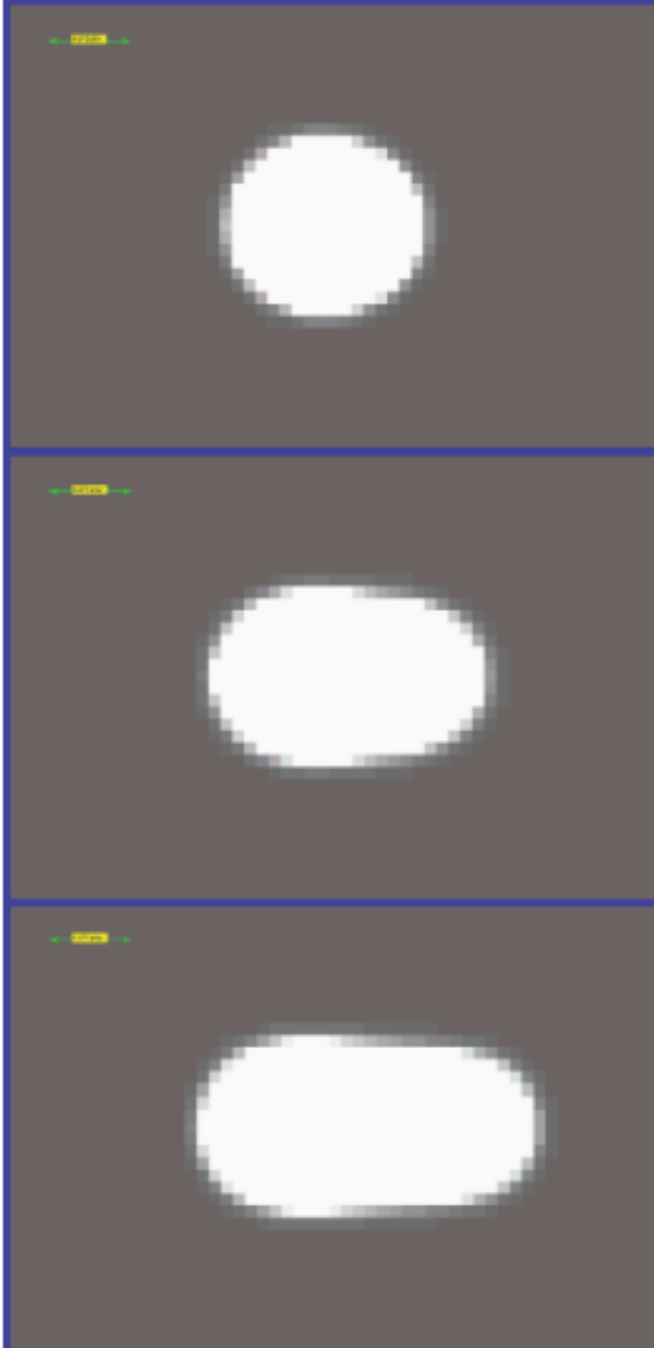
The atmospheric refractive index increases with decreasing wavelength so that blue wavelengths suffer greater refraction than red, leading to dispersion. Dispersion increases rapidly with zenith distance. The plot shows the dispersion as $\sec(Z)$ ranges from 1.1 to 3 airmass (Gemini GMOS web pages)

Differential atmospheric refraction effects are more pronounced at shorter wavelengths and under good seeing conditions.

The effect of differential atmospheric refraction (relative to 500 nm) on Mauna Kea (model) for a point source image with disk seeing of 0.3" and at three different airmasses (1.05, 1.5 and 2.0)

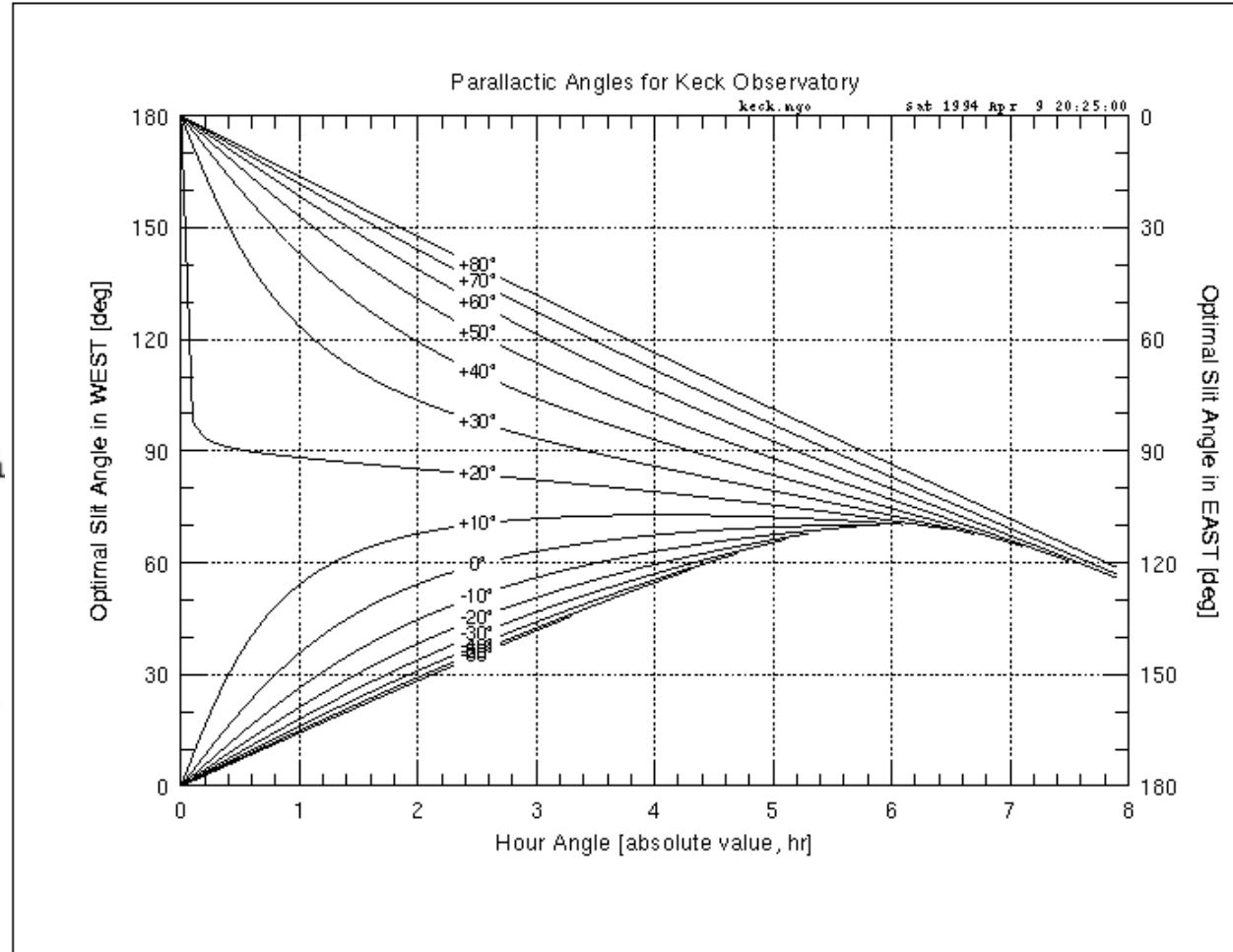
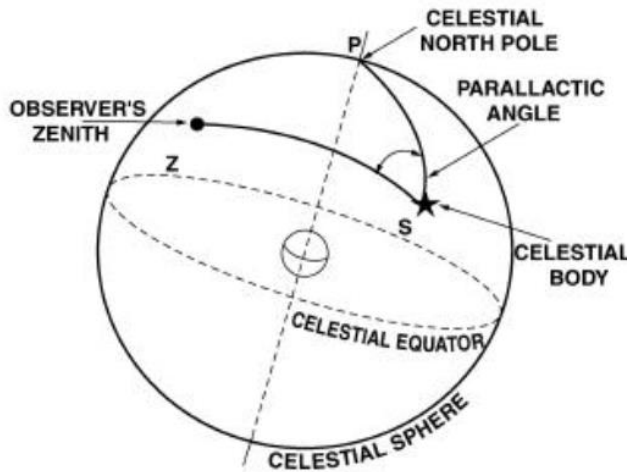
Observations in the g' filter (wavelength range 398-552 nm): the model star looks strongly elongated, particularly at airmasses 1.5 and 2

The effects are much lower in the IR, but may be important for wide-field IR instruments with AO correction



Parallactic Angle for Mauna Kea:

Latitude $19^{\circ} 45' N$



The local vertical angle with respect to North at a particular Declination and Hour Angle

Atmospheric Dispersion Correction

- Many imagers incorporate an Atmospheric Dispersion compensator (a pair of prisms that can be rotated to compensate for dispersion optically)
- Even then, differential refraction and dispersion across the field of wide field instruments may be significant
- Improved image quality and narrow slits require more accurate refraction compensation.
- Careful attention to slit angles is needed to ensure that all wavelengths are admitted by a slit – observations may need to be made at the parallactic angle

Differential Refraction at Paranal

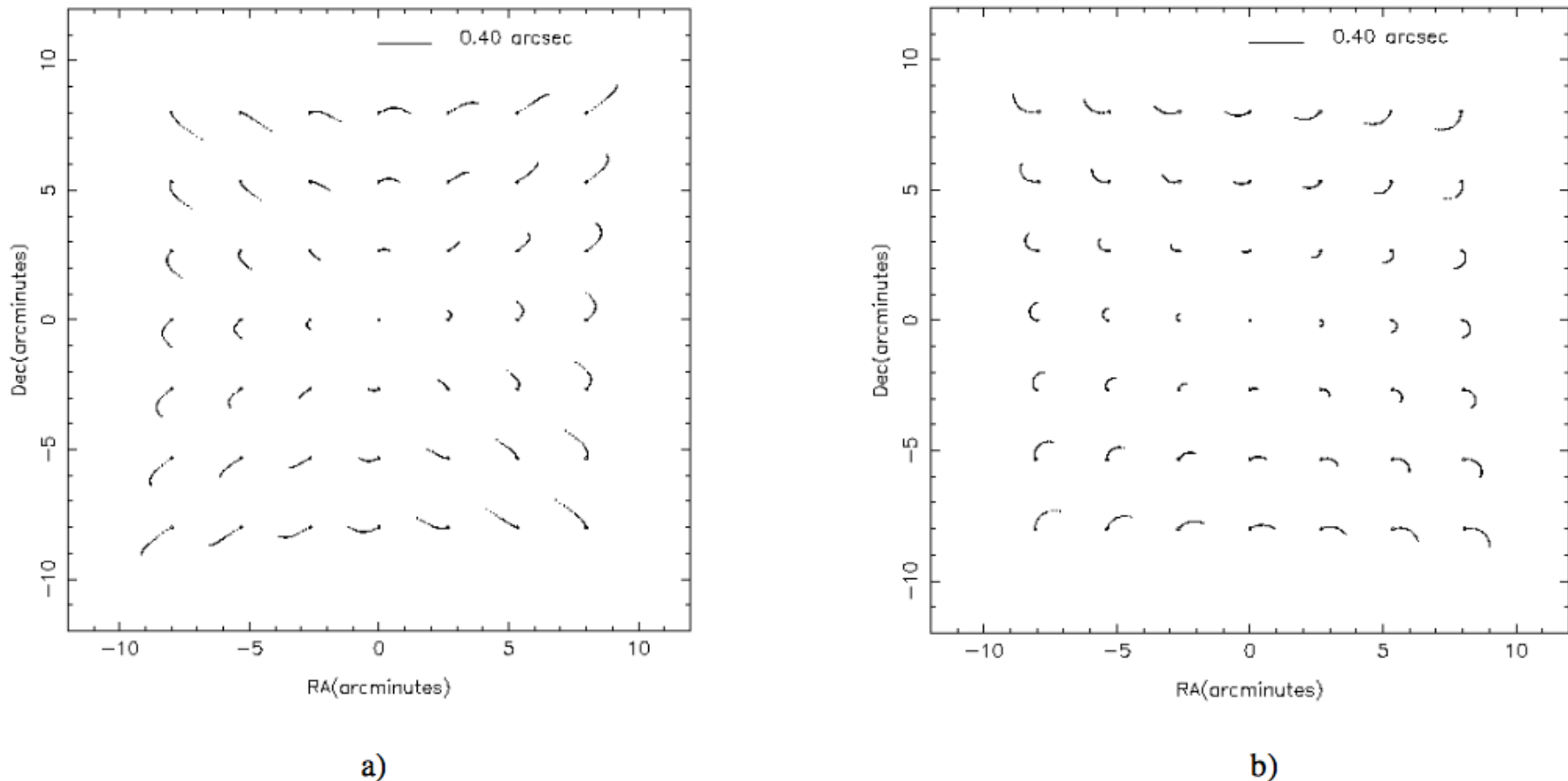


Figure 1. Field differential refraction for a 4 hour exposure starting -2 hours from meridian: a) for a northern object at a +25° declination; b) for a southern object at a -75° declination

The figure shows the differential refraction after field rotation has been compensated for a 16 x 16 arcmin field on Paranal, e.g. for the VIMOS instrument. (J-G Cuby et al)

Wide-field spectroscopy

- Observations with Multi-Object spectrographs in the visible have particular requirements that may affect observation planning
 - Differential refraction across the field changes the mean position of objects over an integration
 - Dispersion is minimised by tracking the parallactic angle
 - But the field on an alt-az telescope rotates
- Some compromise may be needed.
 - Integrations may be split over several nights so that the range of Hour Angle (and thus Parallactic angle variation) is reduced
 - For very wide-field instruments, different slit masks or fibre positions may be needed for observations at different Hour Angles
- Much more detailed treatment of these issues can be found in instrument handbooks or e.g. (Newman P.R. 2002 PASP 114 918).

Radio Frequencies

- $\lambda < 3\text{cm}$ water vapour absorption – need high dry sites
- Between 3cm-50cm atmosphere has little effect on observations (except high winds)
- $\lambda > 50\text{cm}$ ionosphere and solar activity impact observations
- observations at night are preferred
- Refraction in the troposphere:
 - $n_{\text{air}} = 1.00029$ at $T=0^\circ\text{C}$ and $P=760\text{mm}$ of Hg
 - At radio frequencies water vapour increases dielectric constant and has a substantial effect on the refractive index
 - Effect is the same as at shorter wavelengths, but dispersion is not significant
 - Refractive delay is an important factor in interferometry

Refractive delay

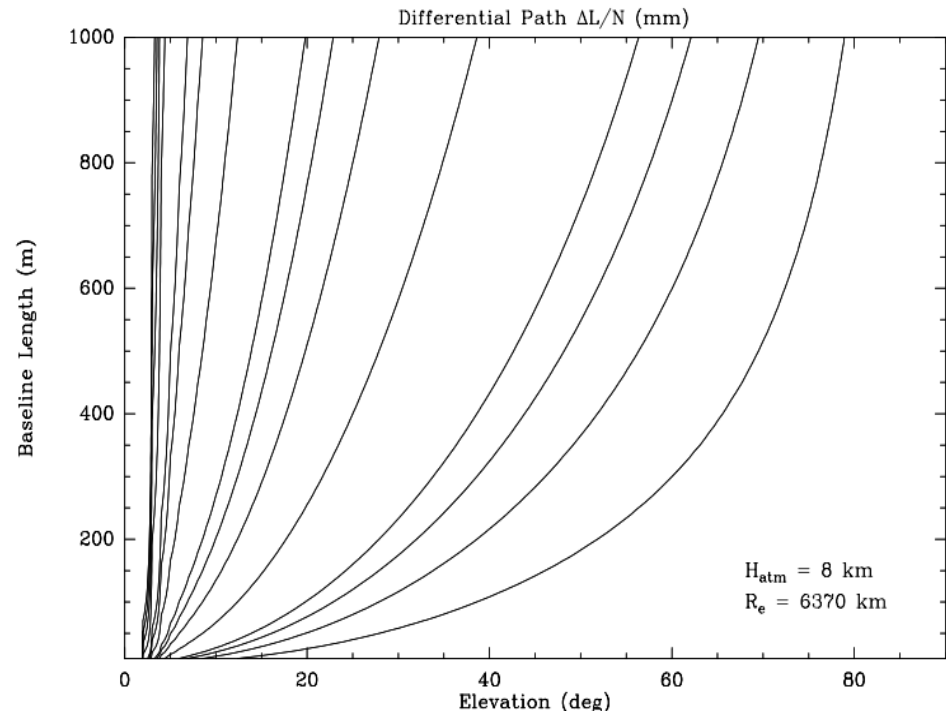
The delay caused by propagation through the atmosphere is the integral of the refractive index along the path

$$t = \int_{r_0}^{\infty} \frac{n(r)}{\sec(z)} dr$$

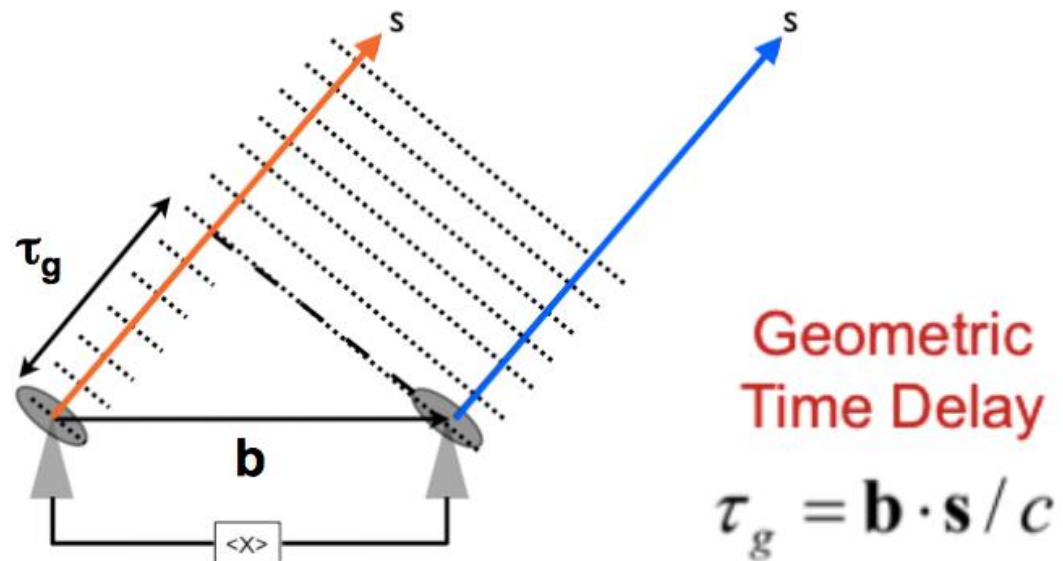
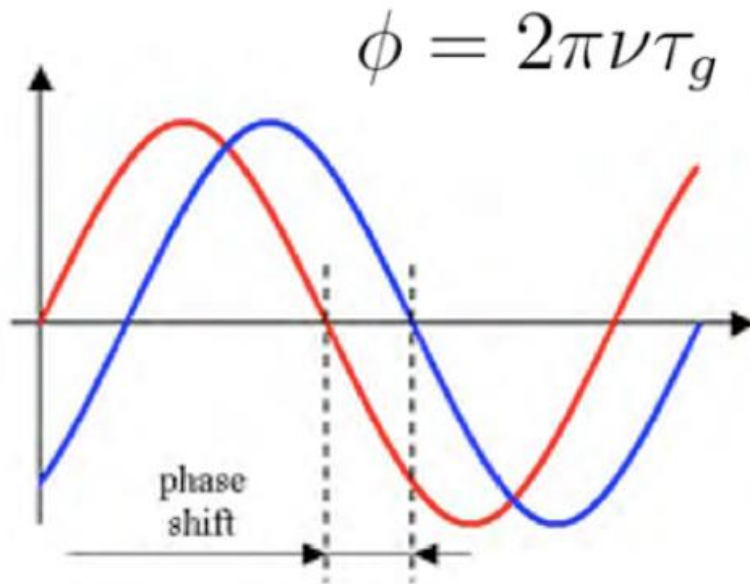
In practice in interferometry, what matters is the differential delay between different telescopes or antennas.

At IR wavelengths, this can amount to many wavelengths, but for most radio telescopes, Δt is rather small

The figure shows contours of delay as a function of baseline and elevation. The contours are 10, 15, 20, 25, 50, 75, 100, 200, 400, 600, 800, 1000, 3000, and 5000 μm from right to left



Interferometer Geometric Delay



The geometric delay that arises from the physical separation of the antennas also has to be factored in.

mm waves

Wavelengths are $\sim 10^3$ times greater than IR, and dishes are only a bit bigger (ALMA antennas are 12-m)

The whole wavefront suffers retardation, but analysis by E Archibald et al (2002) found no evidence for beam broadening due to seeing at the 15-m JCMT on Mauna Kea

Anomalous refraction can lead to image excursions, possibly due to large scale cells moving over the site

ALMA does not seem to suffer from this, probably because the PWV is lower on Chajnantor



ALMA Phase correction

- Water vapour in the troposphere is not well mixed, leading to large variance of total water vapour column along different lines of sight through the atmosphere [SEP]
- Water vapour is usually described in terms of the column of precipitable water vapour (PWV) above the antenna. The PWV at zenith can vary by a factor of 2 above the ALMA site by as much as 50% over a few minutes
- Water vapour has a high effective refractive index, and 1mm of PWV retards the incoming wavefront by about 7mm of path. This is 20λ at ALMA's highest observing frequency
- Radiometers monitor the emission from the 183GHz water vapour line along the line of sight of the observations, providing estimates of the PWV above each antenna.

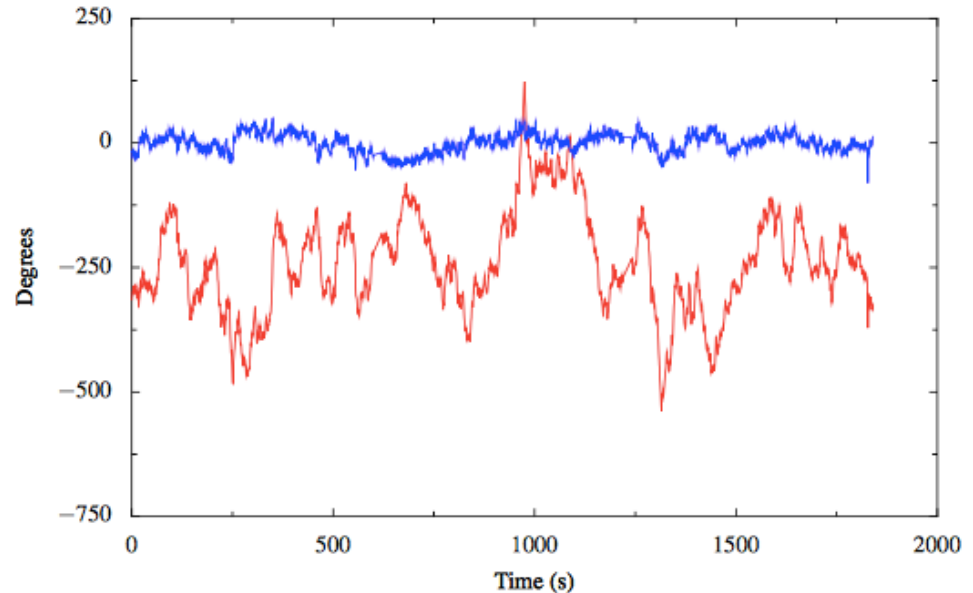


Fig. 8. Test observation at 90 GHz of a strong quasar on a ~650 m baseline with ALMA. The red line is the phase of the observed (complex) visibility on this baseline – note that for a quasar (or other point-like) source at the tracking centre of the interferometer we expect a constant phase in time. The blue line is the visibility phase after correction of the data based on the WVR signals and using the `wvrgcal` program.

Nikolic et al 2013

Space

In space, there is no need to compensate for the atmosphere!!

Diffraction-limited optics take full advantage of unaberrated wavefronts to yield exquisite image quality and sensitivity.

This places severe constraints on the pointing and stability of spacecraft and its payload.

But

Note that the ISM is partially ionized and variations in refractive index can lead to dispersion, scattering and angular broadening at radio frequencies

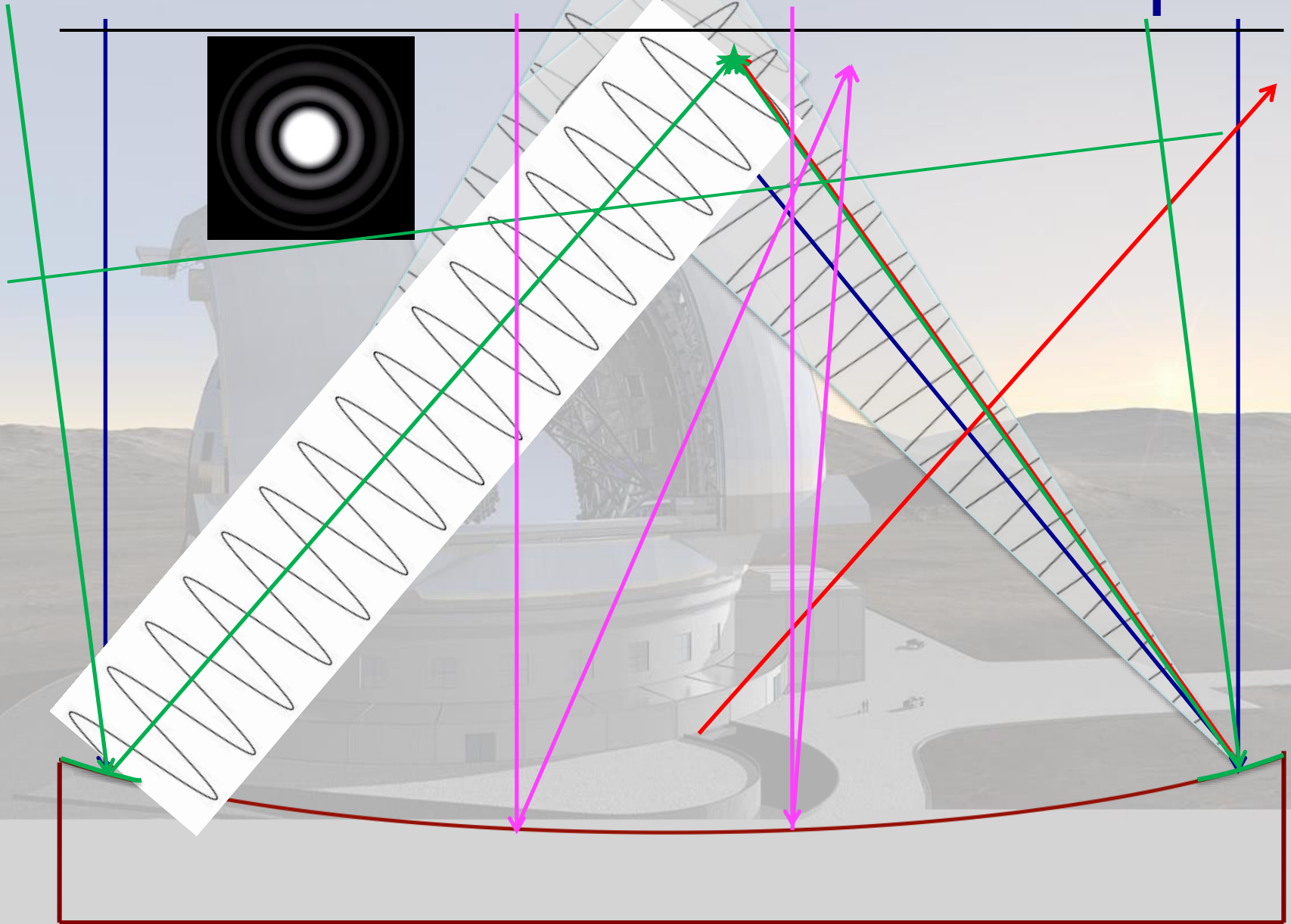
Bigger telescopes yield sharper pictures

- Results from the wave nature of light

Angular resolution = $\frac{\text{wavelength of light}}{\text{Diameter of telescope}}$

$$\theta_0 = 1.22 \frac{\lambda}{D}$$

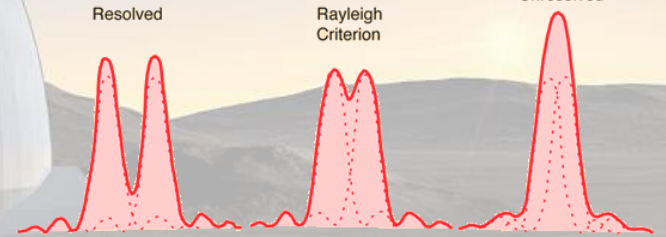
Resolution limit of a telescope



Rayleigh resolution criterion

- Two point sources are said to be resolved when the first minimum of the diffraction pattern of one star overlaps with the peak of the other

image from hyperphysics.phy-astr.gsu.edu

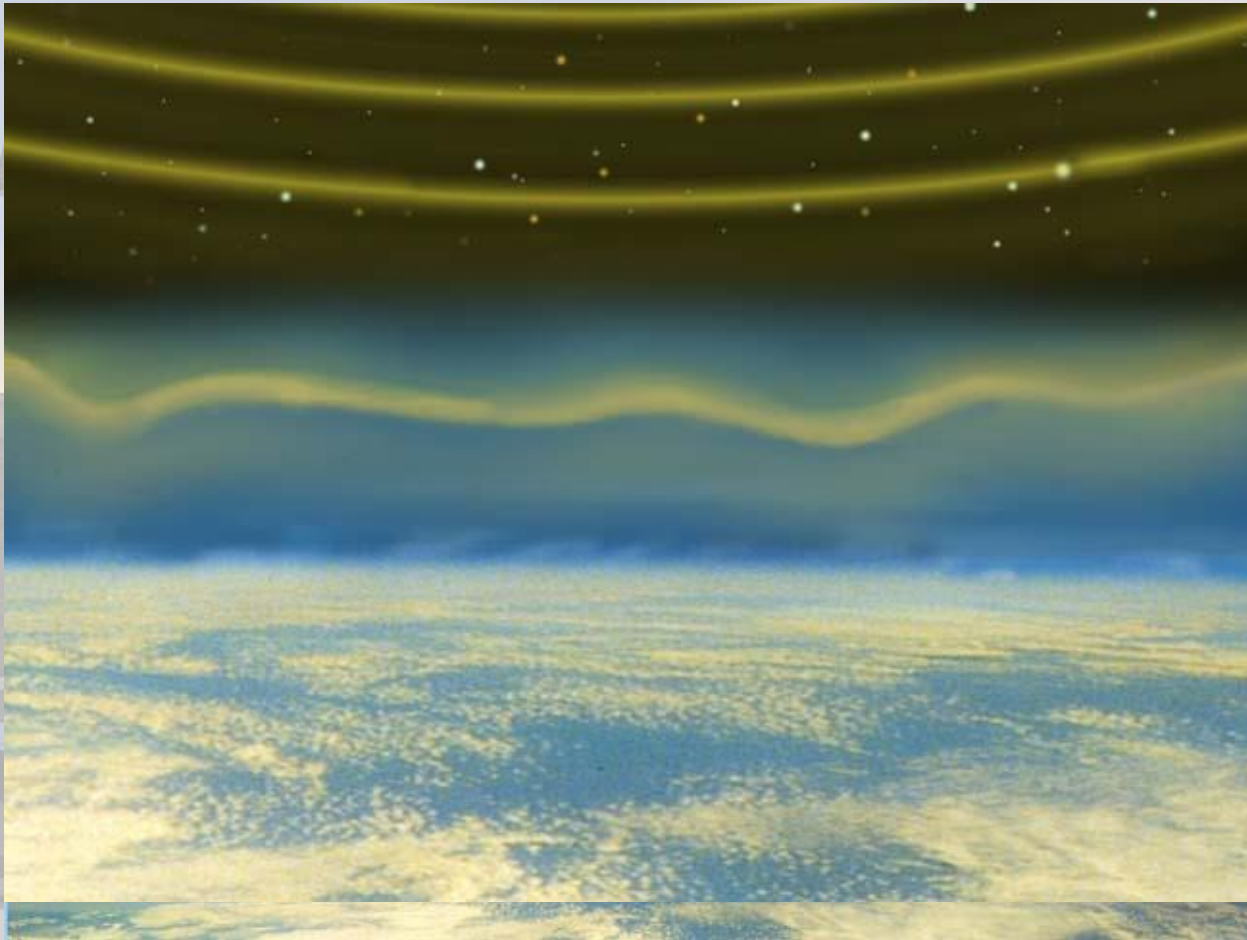


- The first minimum of the Airy pattern occurs at $\theta_{\text{lim}} = 1.22 \lambda / D$
- For $D = 8\text{m}$ and $\lambda = 0.5\mu\text{m}$, $\theta_{\text{lim}} = 0.015$ arcsec!

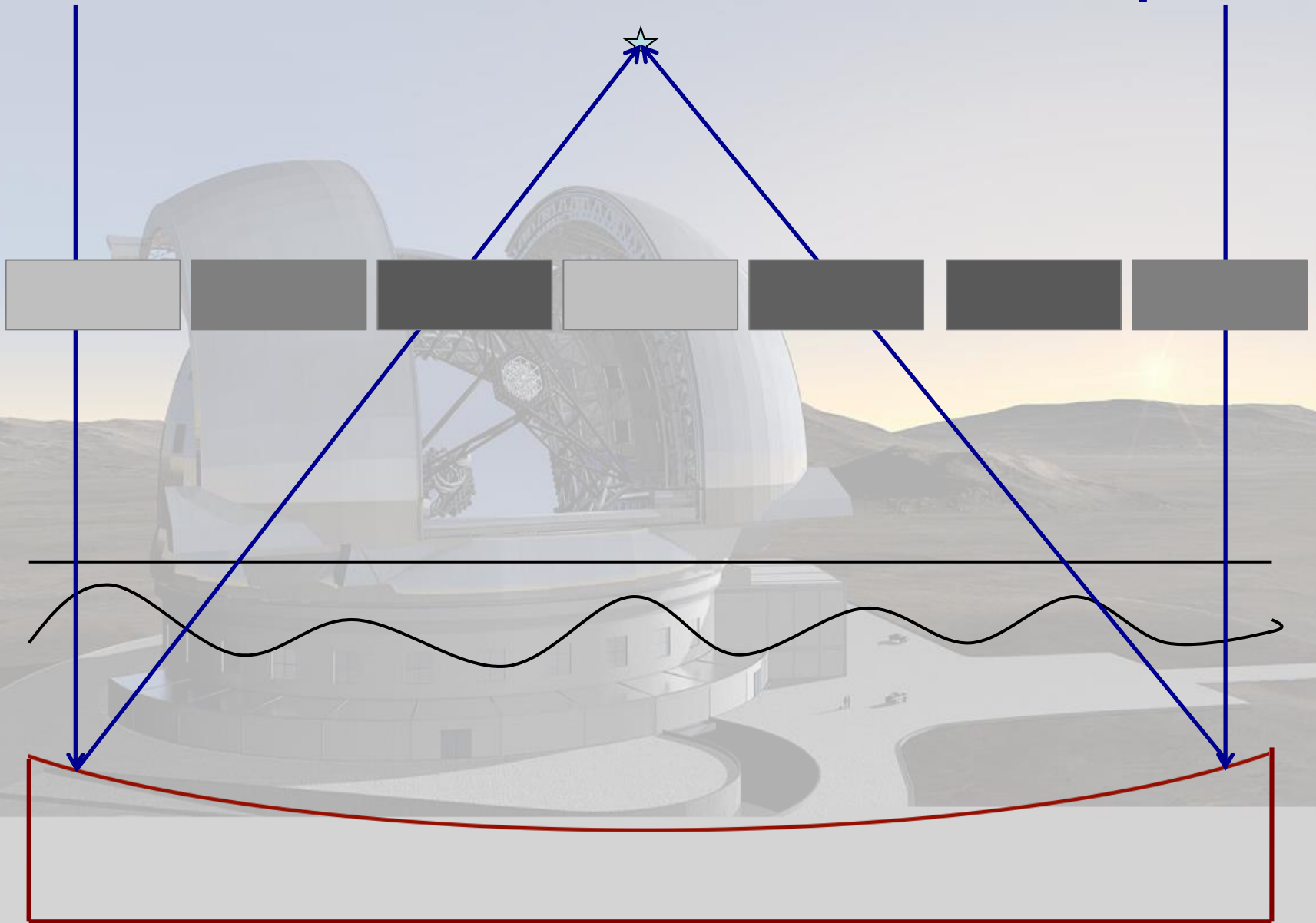
An example



Twinkle, twinkle, little star



Resolution limit of a telescope



Bigger telescopes yield sharper pictures

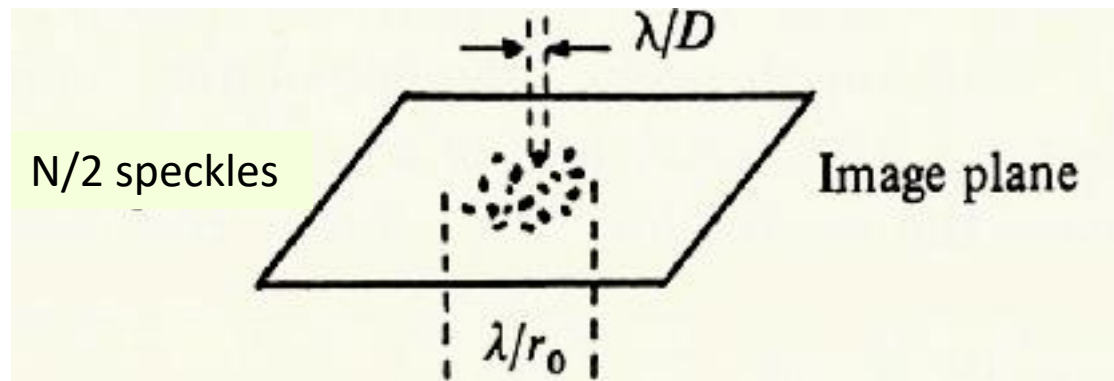
- Results from the wave nature of light

Angular resolution = $\frac{\text{wavelength of light}}{\text{Diameter of telescope}}$

$$\theta_0 = 1.22 \frac{\lambda}{D}$$

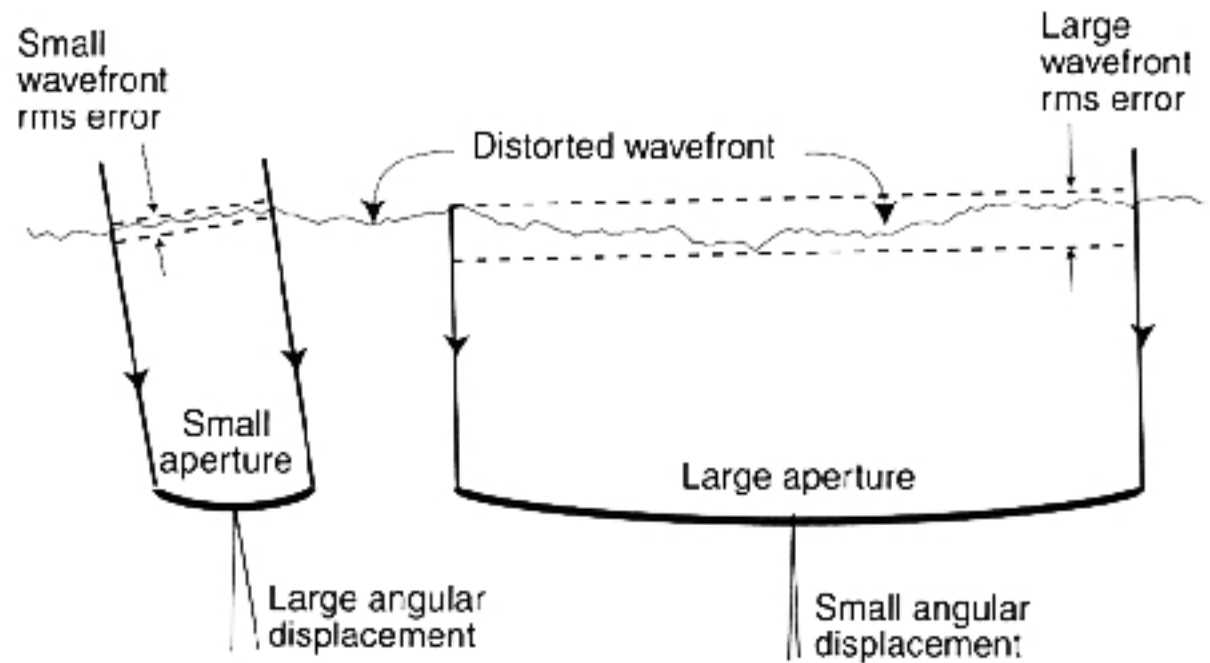
- Ground based telescopes rarely achieve the diffraction limit, as they are limited by turbulence from the earth's atmosphere.

Telescope Image



The telescope pupil contains $N = (D/r_0)^2$ cells of diameter r_0 , which produce speckles of size $\sim \lambda/D$ within the envelope given by the diffraction pattern on a scale λ/r_0 .

Image distortions



When the telescope aperture is similar to r_0 , the dominant distortion will arise from tilts in the wavefront, causing image wander.

Larger apertures encompass many r_0 and so the image will be the sum of many images blurred on a scale of λ/r_0 randomly displaced by the wavefront tilt in the subaperture.

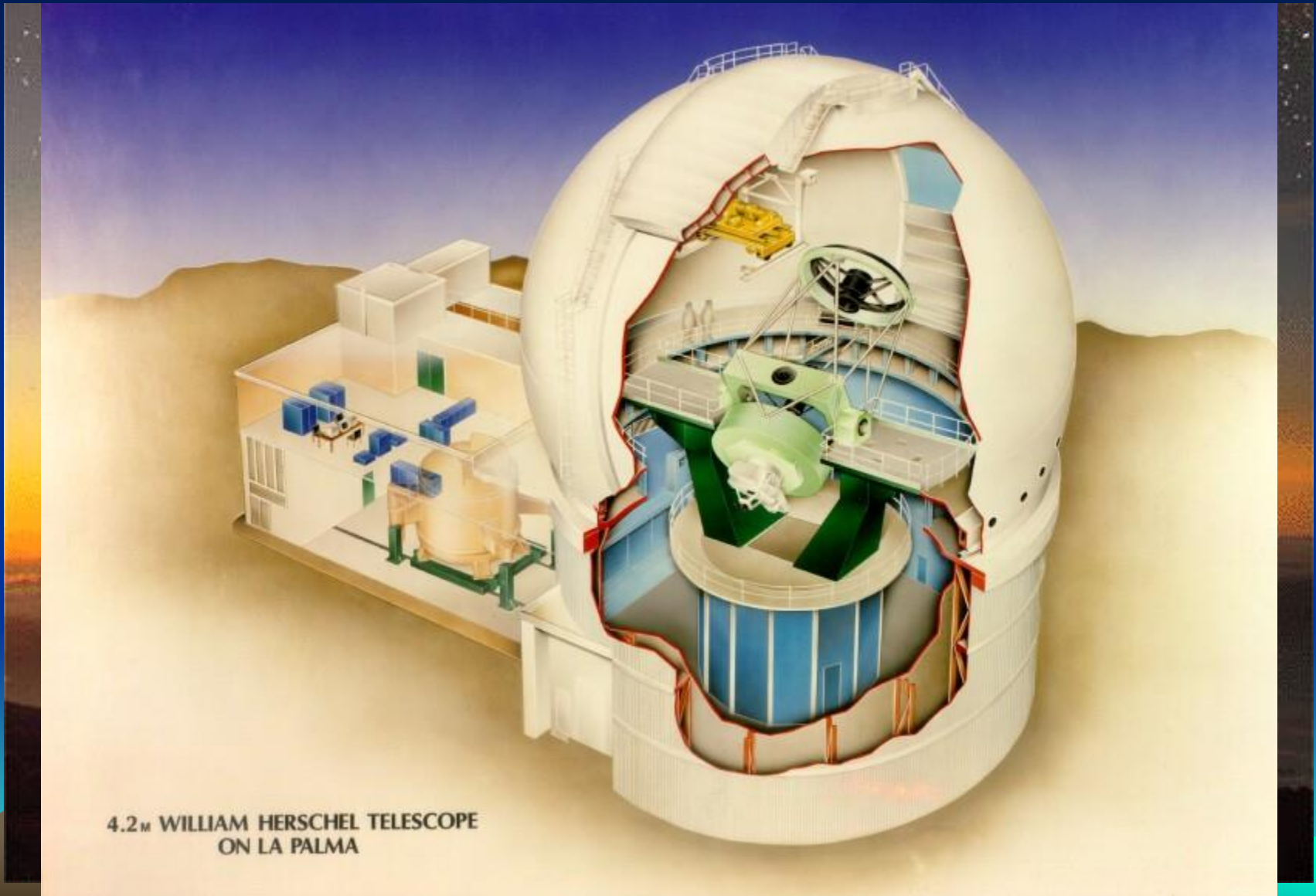
Tip-tilt correction applied to the telescope secondary can (partially) compensate for the overall wavefront tilt, and so is effective at mid-IR wavelengths on 8-m telescopes, near-IR on 4-m telescopes and amateur scale telescopes in the visible.

Similar improvements can be made by using burst mode- many short exposures that are shifted and added, discarding any poor quality images.

Or by using "Lucky Imaging", selecting only the highest quality images for coaddition. Both of these techniques impose significant overheads on the observations.

(Figure from Bely)

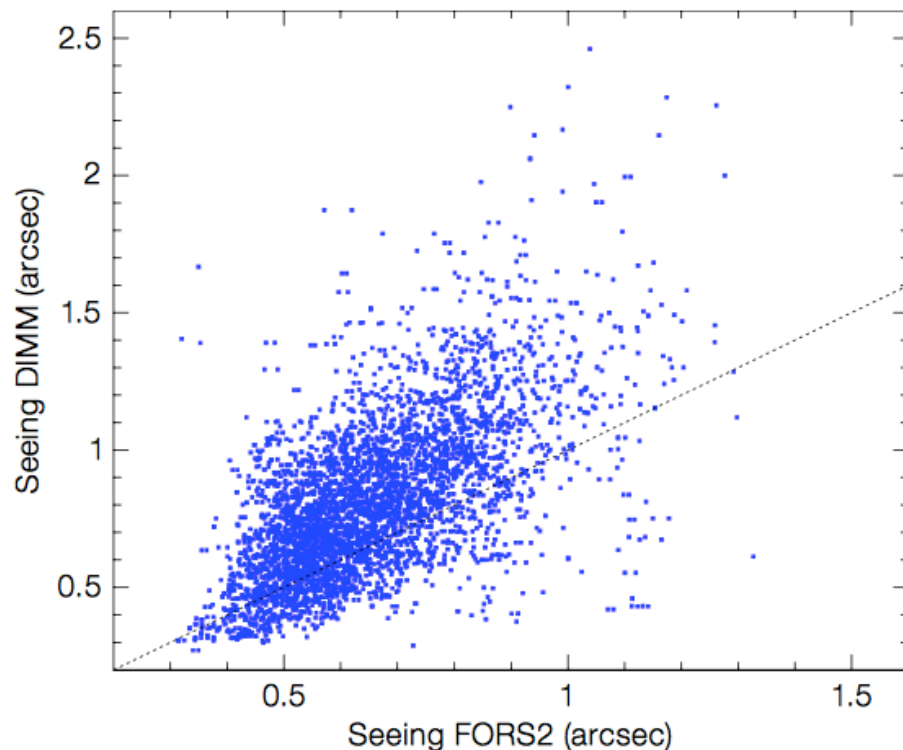
Dome seeing and ground layer



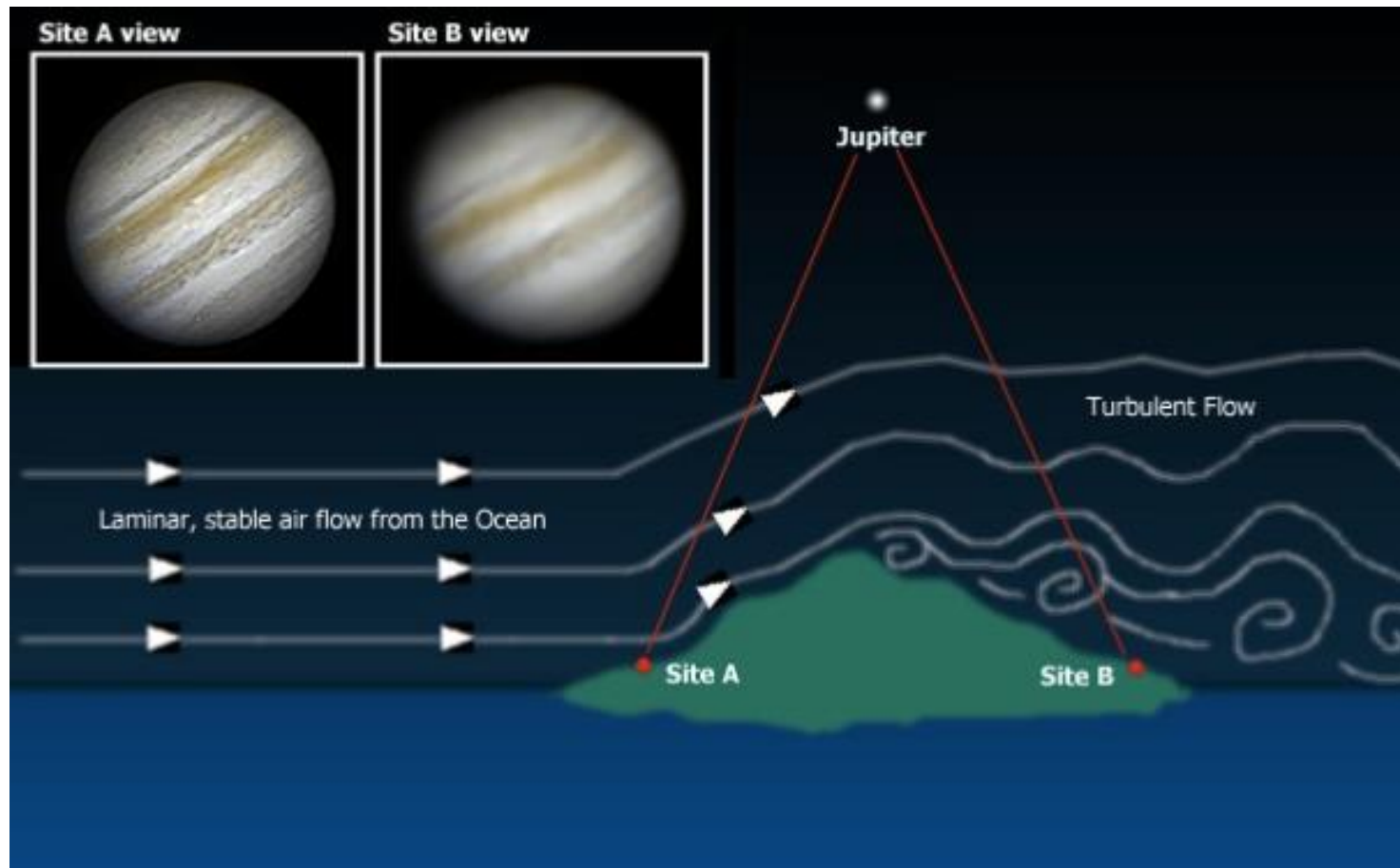
Seeing

- Turbulence along the whole path through the atmosphere contributes to the seeing
 - Jet stream can produce very fast winds, rapid changes and short coherence times
 - Local heating or topography from the mountain or the telescope dome can generate additional turbulence over the free-air profile - ground layer turbulence
 - Seeing may be seasonal or depend on wind directions etc

Many sites monitor seeing in real time using a DIMM (Differential Image Motion Monitor), but for accurate measurements the DIMM should be colocated and at the same altitude as the primary mirror

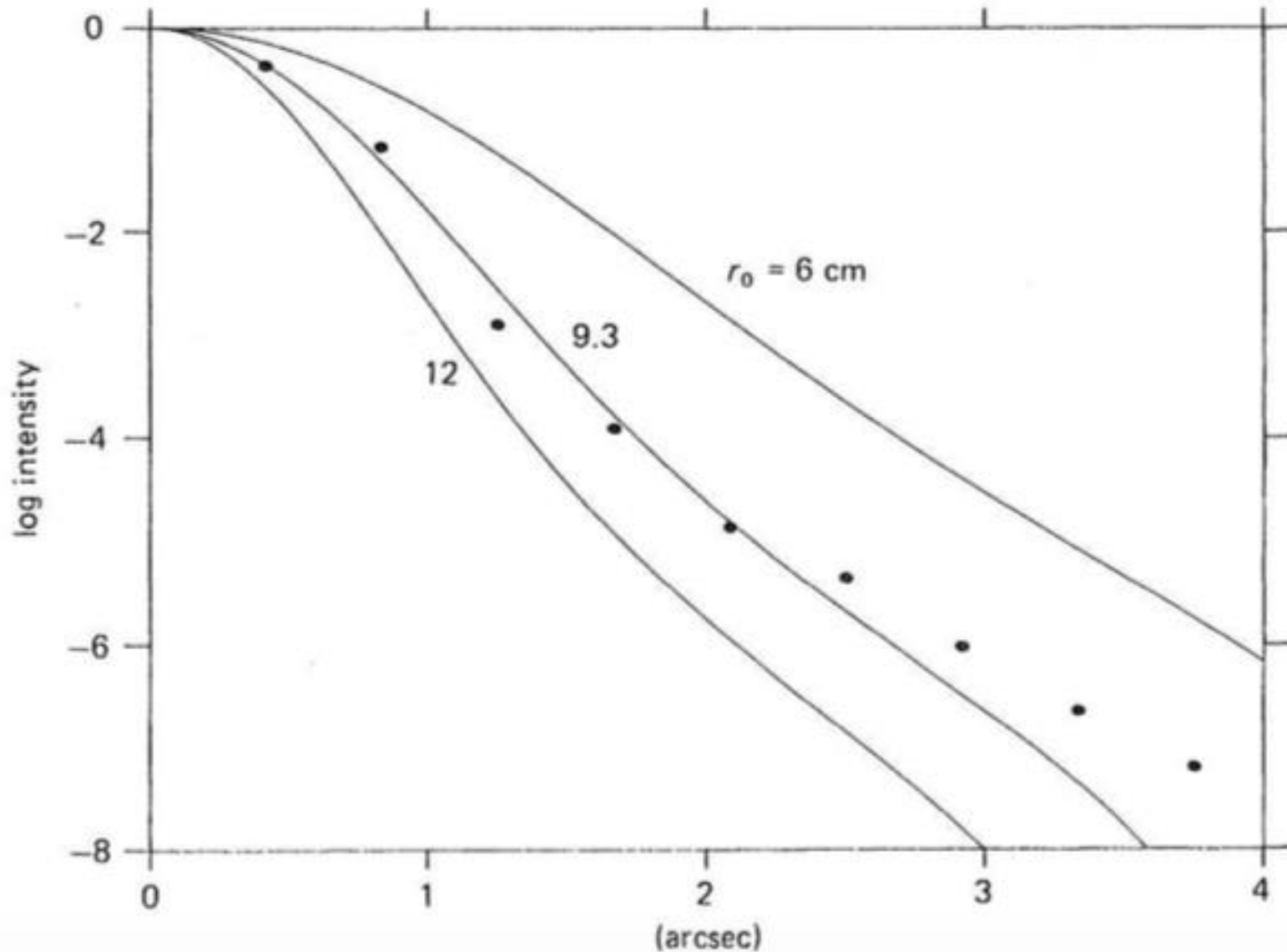


Effects of atmospheric turbulence - seeing



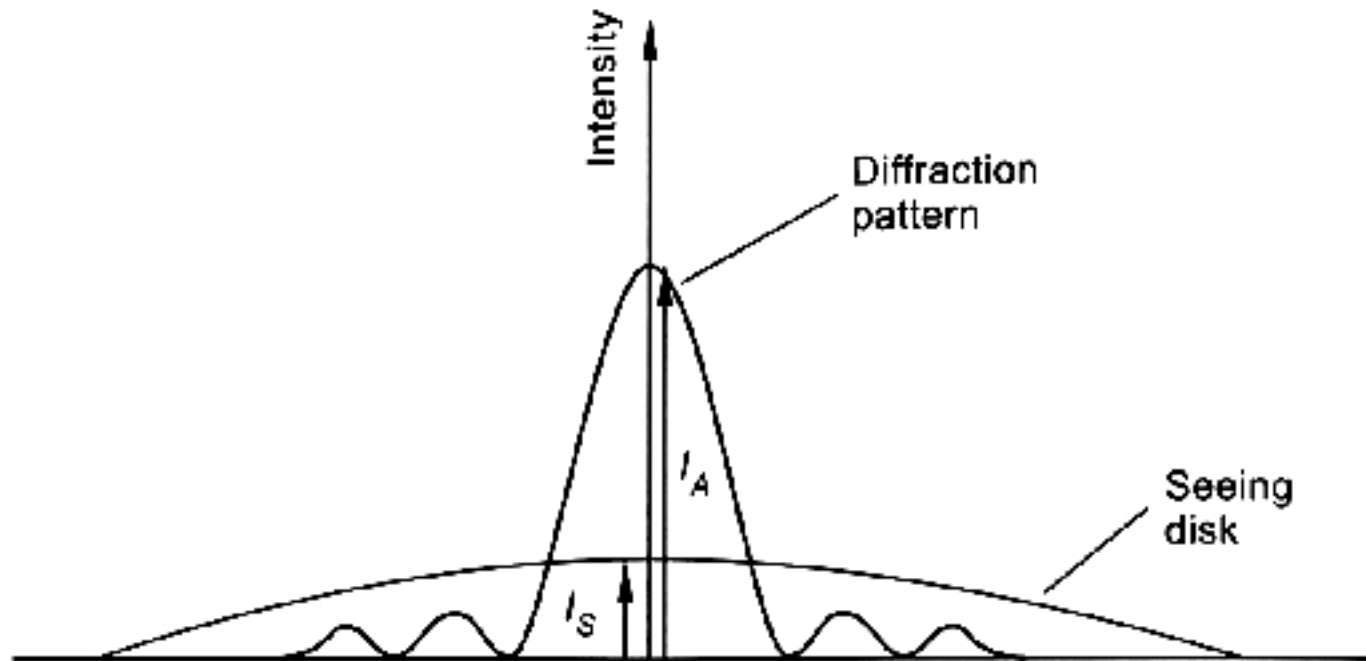
Seeing-limited images

- In long exposures, the speckle component averages out, and the resultant image is the accumulated integration of the images of size λ/r_0
- The resulting images typically have a near-gaussian core set by the transfer function of the atmosphere.
- However at large angles (>5 arcsec), scattering from mirror imperfections (scratches, splodges etc) lead to a halo which is brighter than expected for diffraction alone.
- Note that because of the wavelength dependence of seeing, stars of different colours will have slightly different profiles in wide-band images.



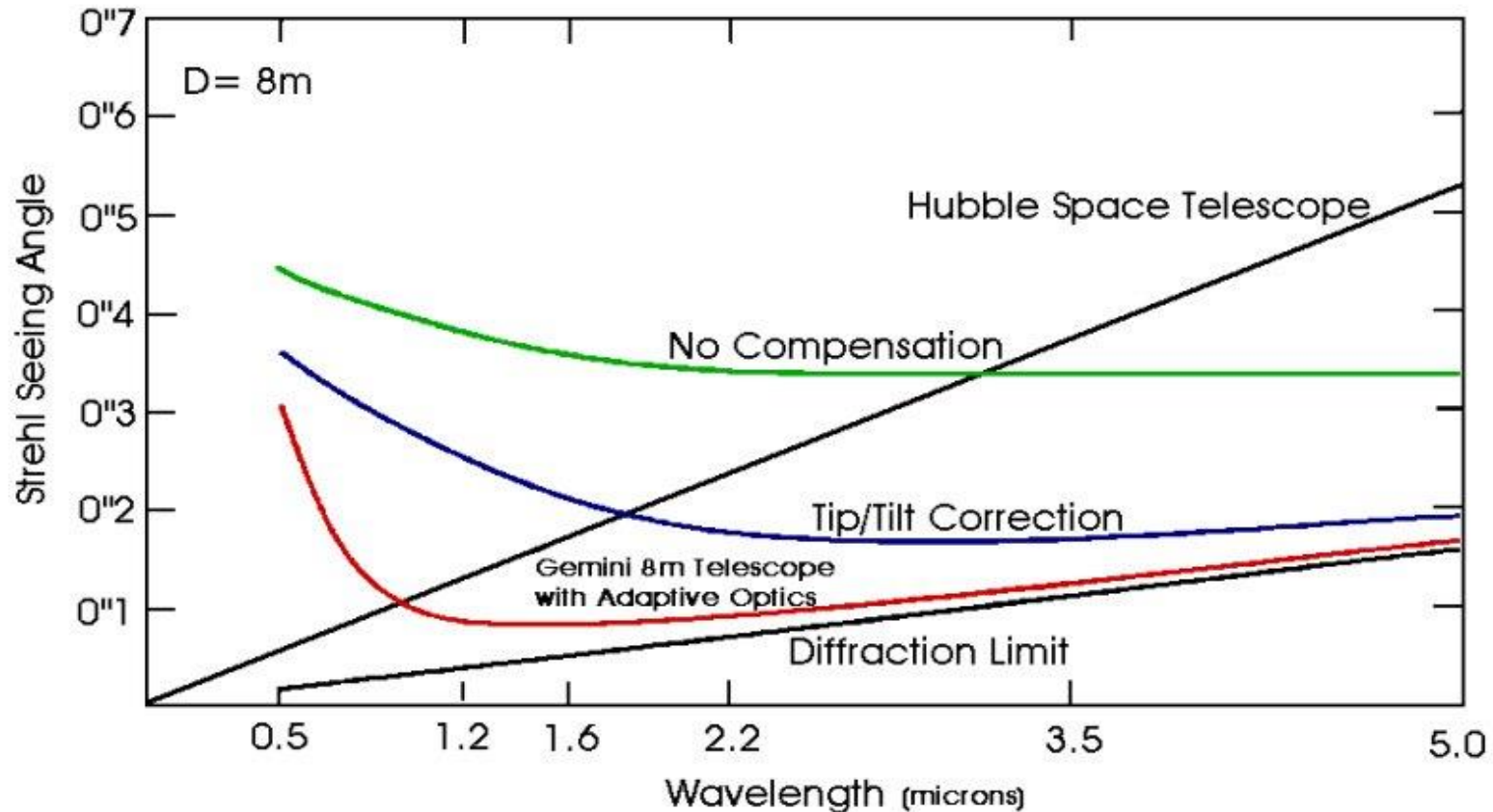
Theoretical long exposure image profiles for 3 different values of r_0 compared with observations (points) made in average seeing conditions at V with the CFHT on Mauna Kea. The departure beyond 3 arcsec probably represents the mirror scattering component (G Walker 1989)

Strehl Ratio



The ratio of the peak intensity of the measured image to that calculated from the diffraction pattern of the telescope optics is the Strehl Ratio

Wavelength dependence

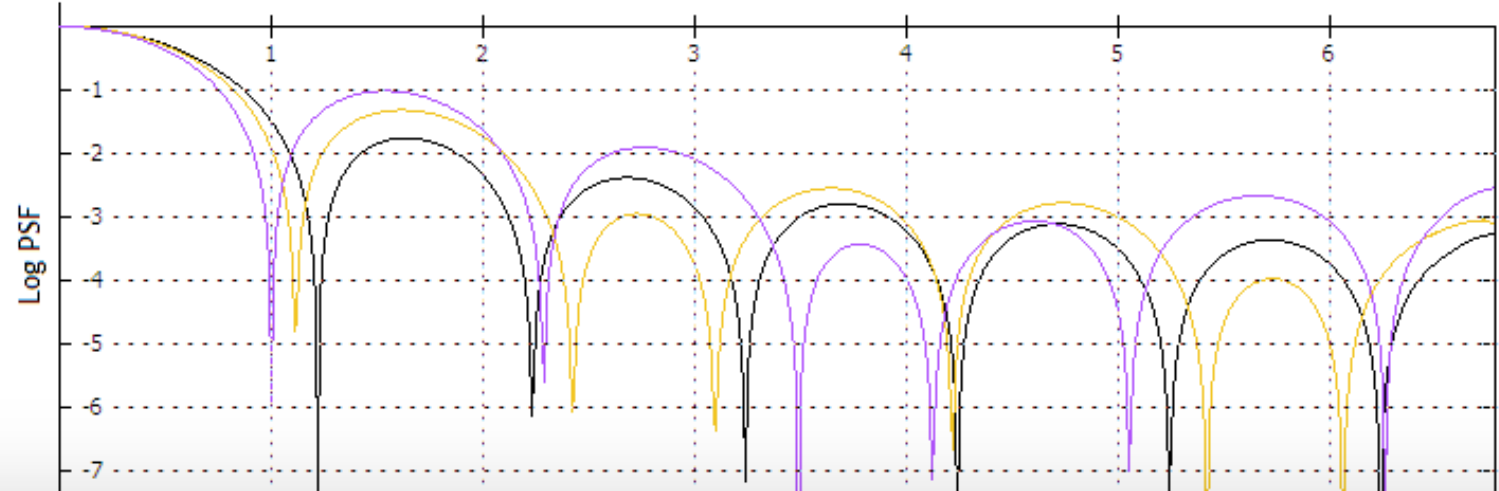
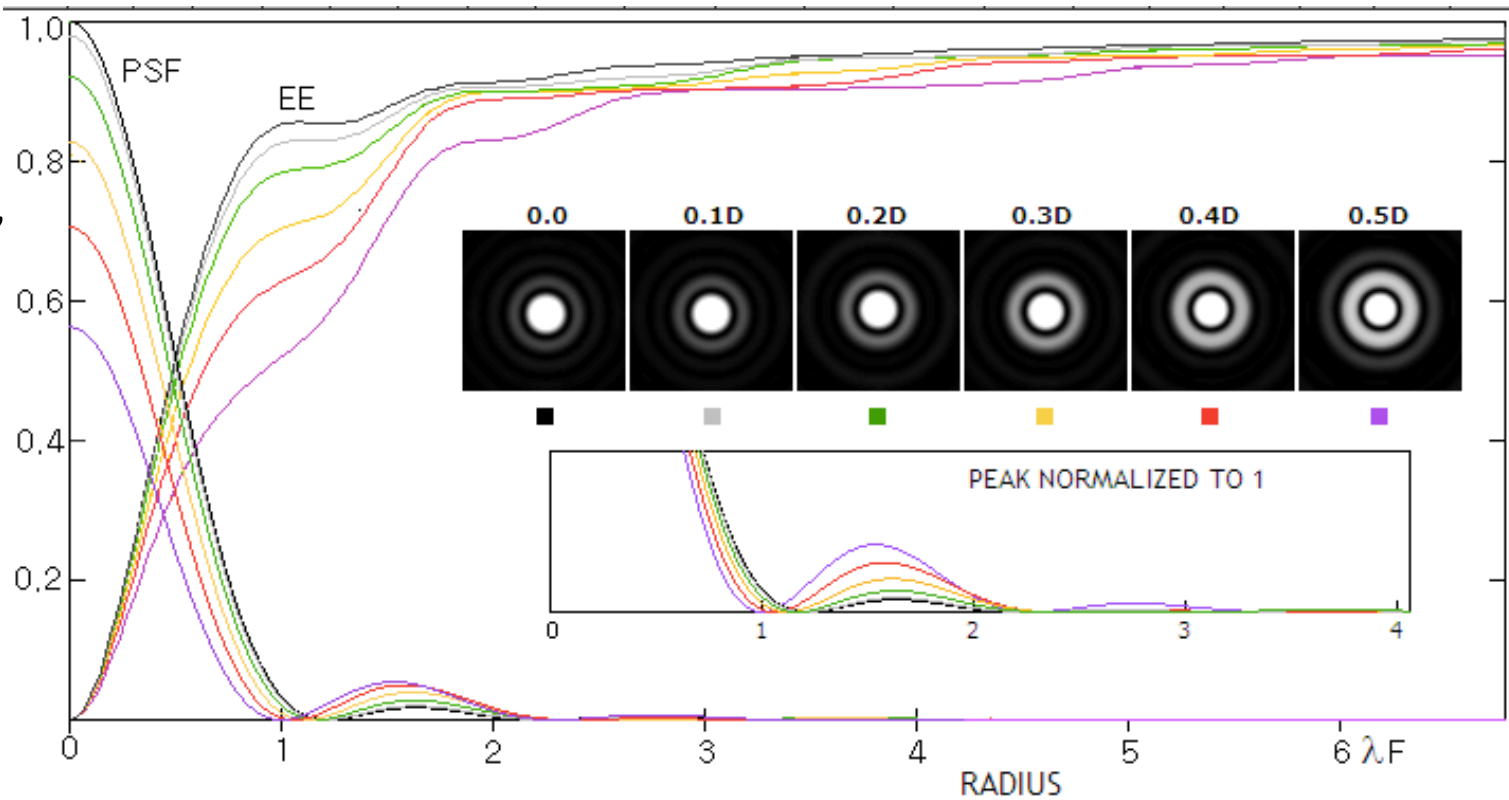


- To a good approximation, atmospheric turbulence follows a Kolmogorov spectrum, with the coherence scale
$$r_0(\lambda) \sim r_0(\lambda_0) (\lambda/\lambda_0)^{1.2} (\cos(z))^{0.6}.$$
- so that the seeing disk in the IR is smaller than in the visible : $\text{FWHM} \propto \lambda^{-0.2}$
- At $2\mu\text{m}$ it is 0.75 times that at $0.5\mu\text{m}$, and at $10\mu\text{m}$ it is 0.55.

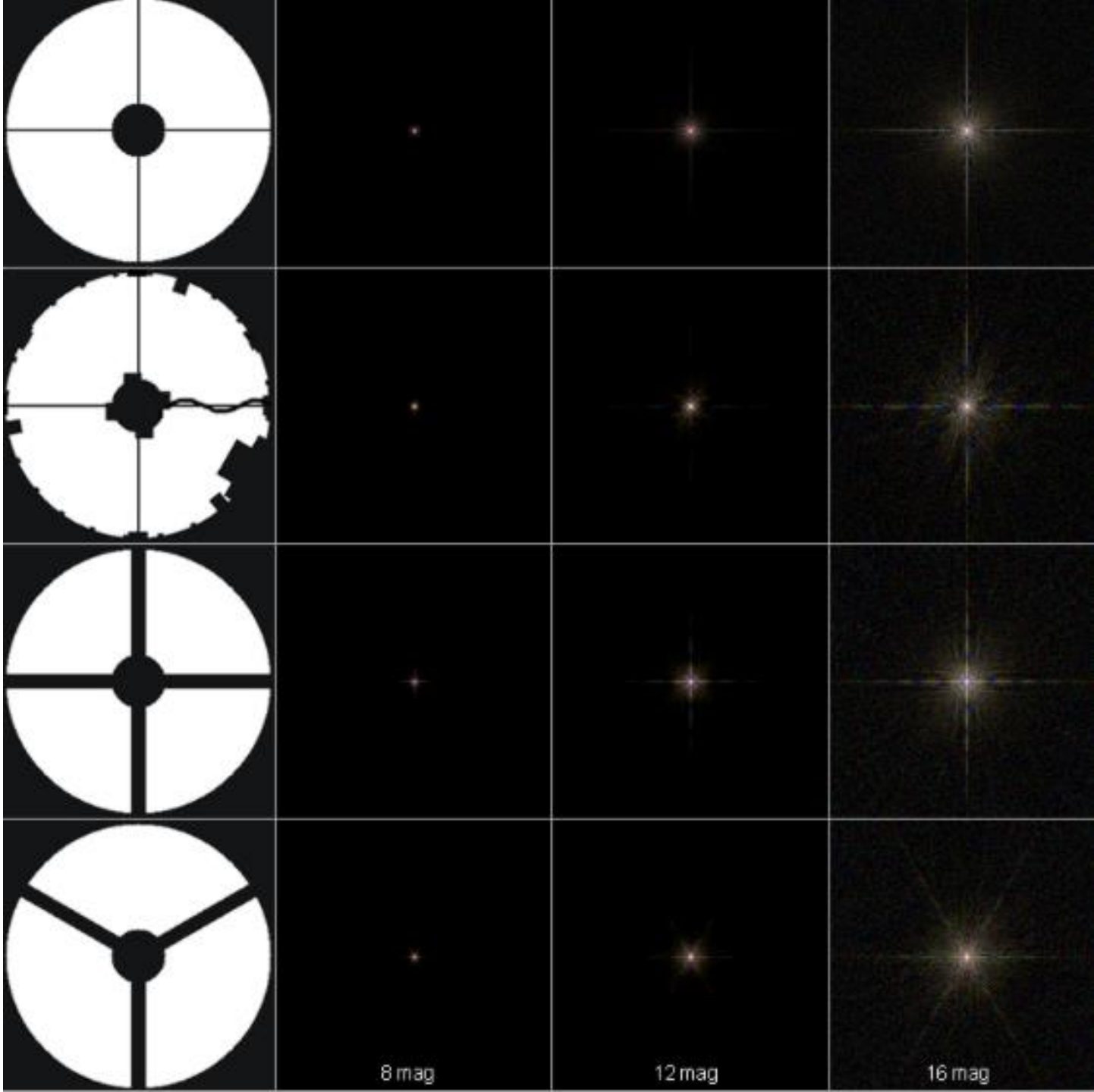
Effect of the Telescope Central Obstruction

pushes more power into the diffraction rings, but also narrows the central maximum

It also reduces the flux collected and produces greater discontinuities in the wavefront in the telescope pupil



- The point spread function delivered by the telescope depends on the mirror surfaces and alignment, the atmosphere and the effects of the central obstruction and secondary mirror vanes on the telescope pupil.



R Pascal

Coherence time

- The simplest model assumes that the turbulent atmosphere is blown across the telescope aperture by the wind.
- In this case, the characteristic (Greenwood) frequency of the atmosphere can be approximated by:
- $f_G = 0.43 V_{\text{wind}}/r_0$ which, with $r_0 \sim \lambda^{1.2}$, means that the coherence time, $t_0 \sim \lambda^{1.2}$ and is in the range ~ 2 to 20msec from the visible to the IR.
- The frame time to freeze the atmosphere is longer at IR wavelengths while the number of r_0 subapertures in the telescope pupil is smaller
- At long wavelengths, r_0 can approach the size of the telescope aperture and low order correction will be effective. At shorter wavelengths, higher order correction – Adaptive Optics – is required.

Shift and Add can sharpen images

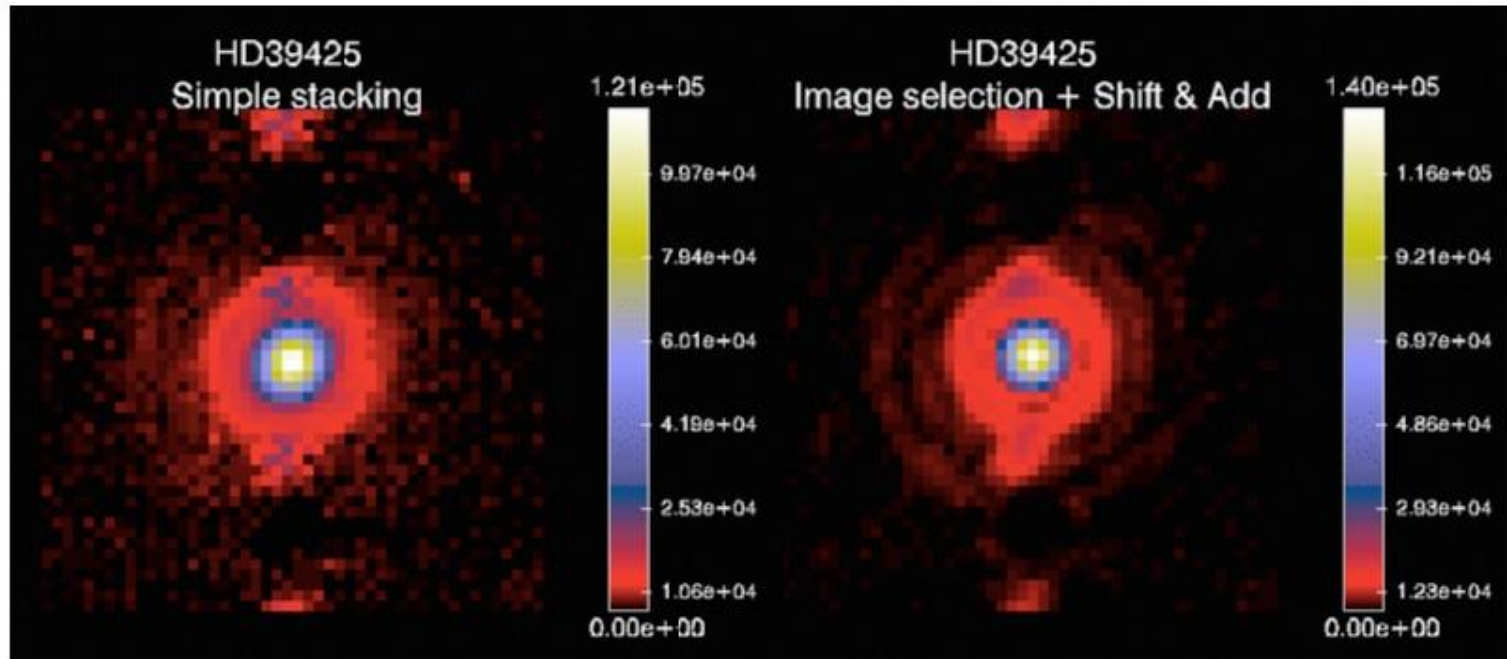


Figure 5. Left panel : simple stack of burst mode frames of the standard star HD39425, simulating a classical observation. Right panel, shift-and-add and image selection are applied to burst mode data. The average FWHM is decreased by 15% and the Strehl ratio is improved from 0.52 to 0.65. Note also the two unveiled diffraction rings (dark red) appearing in right panel.

Images with VISIR on the VLT demonstrate the improvements obtained with shift and add